Received: 24 September 2013 Accepted: 12 December 2013
Published: 21 December 2013

References

1. Fischer J, Lefevre C, Morava E, Mussini JM, Laforet P, Negre-Salvayre A, Lathrop M, Salvayre R: **The gene encoding adipose triglyceride lipase (PNPLA2) is mutated in neutral lipid storage disease with myopathy.** *Nat Genet* 2007, **39**:28–30.
2. Schweiger M, Lass A, Zimmermann R, Eichmann TO, Zechner R: **Neutral lipid storage disease: genetic disorders caused by mutations in adipose triglyceride lipase/PNPLA2 or CGI-58/ABHD5.** *Am J Physiol Endocrinol Metab* 2009, **297**:E289–E296.
3. Ong KT, Mashek MT, Bu SY, Greenberg AS, Mashek DG: **Adipose triglyceride lipase is a major hepatic lipase that regulates triacylglycerol turnover and fatty acid signaling and partitioning.** *Hepatology* 2011, **53**:116–126.
4. Smirnova E, Goldberg EB, Makarova KS, Lin L, Brown WJ, Jackson CL: **ATGL has a key role in lipid droplet/adiposome degradation in mammalian cells.** *EMBO Rep* 2006, **7**:106–113.
5. Reilich P, Horvath R, Krause S, Schramm N, Turnbull DM, Trenell M, Hollingsworth KG, Gorman GS, Hans VH, Reimann J, *et al*: **The phenotypic spectrum of neutral lipid storage myopathy due to mutations in the PNPLA2 gene.** *J Neurol* 2011, **258**:1987–1997.
6. Hirano K, Ikeda Y, Zaima N, Sakata Y, Matsumiya G: **Triglyceride deposit cardiomyovasculopathy.** *N Engl J Med* 2008, **359**:2396–2398.
7. Hirano K: **A novel clinical entity: triglyceride deposit cardiomyovasculopathy.** *J Atheroscler Thromb* 2009, **16**:702–705.
8. Ong SE, Blagoev B, Kratchmarova I, Kristensen DB, Steen H, Pandey A, Mann M: **Stable isotope labeling by amino acids in cell culture, SILAC, as a simple and accurate approach to expression proteomics.** *Mol Cell Proteomics* 2002, **1**:376–386.
9. Muraoka S, Kume H, Watanabe S, Adachi J, Kuwano M, Sato M, Kawasaki N, Kodera Y, Ishitobi M, Inaji H, *et al*: **Strategy for SRM-based verification of biomarker candidates discovered by iTRAQ method in limited breast cancer tissue samples.** *J Proteome Res* 2012, **11**:4201–4210.
10. Rappsilber J, Mann M, Ishihama Y: **Protocol for micro-purification, enrichment, pre-fractionation and storage of peptides for proteomics using StageTips.** *Nat Protoc* 2007, **2**:1896–1906.
11. Cox J, Mann M: **MaxQuant enables high peptide identification rates, individualized p.p.b.-range mass accuracies and proteome-wide protein quantification.** *Nat Biotechnol* 2008, **26**:1367–1372.
12. Masuda T, Tomita M, Ishihama Y: **Phase transfer surfactant-aided trypsin digestion for membrane proteome analysis.** *J Proteome Res* 2008, **7**:731–740.
13. Linton K, Howarth C, Wappett M, Newton G, Lachel C, Iqbal J, Pepper S, Byers R, Chan WJ, Radford J: **Microarray gene expression analysis of fixed archival tissue permits molecular classification and identification of potential therapeutic targets in diffuse large B-cell lymphoma.** *J Mol Diagn* 2012, **14**:223–232.
14. Johansson A, Curran JE, Johnson MP, Freed KA, Fenstad MH, Bjorge L, Eide IP, Carless MA, Rainwater DL, Goring HH, *et al*: **Identification of ACOX2 as a shared genetic risk factor for preeclampsia and cardiovascular disease.** *Eur J Hum Genet* 2011, **19**:796–800.
15. Prasad P, Tiwari AK, Kumar KM, Ammini AC, Gupta A, Gupta R, Thelma BK: **Association analysis of ADPRT1, AKR1B1, RAGE, GFPT2 and PAI-1 gene polymorphisms with chronic renal insufficiency among Asian Indians with type-2 diabetes.** *BMC Med Genet* 2010, **11**:52.
16. Kirino Y, Sato Y, Kamimoto T, Kawazoe K, Minakuchi K, Nakahori Y: **Interrelationship of dipeptidyl peptidase IV (DPP4) with the development of diabetes, dyslipidaemia and nephropathy: a streptozotocin-induced model using wild-type and DPP4-deficient rats.** *J Endocrinol* 2009, **200**:53–61.
17. Waterham HR, Koster J, Romeijn GJ, Hennekam RC, Vreken P, Andersson HC, FitzPatrick DR, Kelley RI, Wanders RJ: **Mutations in the 3beta-hydroxysterol Delta24-reductase gene cause desmosterolosis, an autosomal recessive disorder of cholesterol biosynthesis.** *Am J Hum Genet* 2001, **69**:685–694.
18. Bruins Slot MH, Reitsma JB, Rutten FH, Hoes AW, van der Heijden GJ: **Heart-type fatty acid-binding protein in the early diagnosis of acute myocardial infarction: a systematic review and meta-analysis.** *Heart* 2010, **96**:1957–1963.
19. Fortunato G, Di Taranto MD, Bracale UM, Del Guercio L, Carbone F, Mazzaccara C, Morgante A, D'Armiento FP, D'Armiento M, Porcellini M, *et al*: **Decreased paraoxonase-2 expression in human carotids during the progression of atherosclerosis.** *Arterioscler Thromb Vasc Biol* 2008, **28**:594–600.
20. Lattka E, Illig T, Koletzko B, Heinrich J: **Genetic variants of the FADS1 FADS2 gene cluster as related to essential fatty acid metabolism.** *Curr Opin Lipidol* 2010, **21**:64–69.
21. Stattermayer AF, Rutter K, Beinhardt S, Wrba F, Scherzer TM, Strasser M, Hofer H, Steindl-Munda P, Trauner M, Ferenci P: **Role of FDFT1 polymorphism for fibrosis progression in patients with chronic hepatitis C.** *Liver Int* 2013. Epub ahead of print.
22. Chang BH, Chan L: **Regulation of Triglyceride Metabolism. III. Emerging role of lipid droplet protein ADFP in health and disease.** *Am J Physiol Gastrointest Liver Physiol* 2007, **292**:G1465–G1468.
23. Simmons DL: **Variants of cyclooxygenase-1 and their roles in medicine.** *Thromb Res* 2003, **110**:265–268.
24. Adiguzel E, Hou G, Sabatini PJ, Bendeck MP: **Type VIII collagen signals via beta1 integrin and RhoA to regulate MMP-2 expression and smooth muscle cell migration.** *Matrix Biol* 2013, **32**:332–341.
25. Pan TC, Zhang RZ, Markova D, Arita M, Zhang Y, Bogdanovich S, Khurana TS, Bonnemann CG, Birk DE, Chu ML: **COL6A3 protein deficiency in mice leads to muscle and tendon defects similar to human collagen VI congenital muscular dystrophy.** *J Biol Chem* 2013, **288**:14320–14331.
26. Seppinen L, Pihlajaniemi T: **The multiple functions of collagen XVIII in development and disease.** *Matrix Biol* 2011, **30**:83–92.
27. Stohn JP, Perreault NG, Wang Q, Liaw L, Lindner V: **Cthrc1, a novel circulating hormone regulating metabolism.** *PLoS One* 2012, **7**:e47142.
28. Straub BK, Gyoengyoesi B, Koenig M, Hashani M, Pawella LM, Herpel E, Mueller W, Macher-Goeppinger S, Heid H, Schirmacher P: **Adipophilin/perilipin-2 as a lipid droplet-specific marker for metabolically active cells and diseases associated with metabolic dysregulation.** *Histopathology* 2013, **62**:617–631.
29. Sandilands A, Sutherland C, Irvine AD, McLean WH: **Filaggrin in the frontline: role in skin barrier function and disease.** *J Cell Sci* 2009, **122**:1285–1294.
30. Campoli M, Ferrone S, Wang X: **Functional and clinical relevance of chondroitin sulfate proteoglycan 4.** *Adv Canc Res* 2010, **109**:73–121.
31. Ducros E, Berthaut A, Mirshahi P, Lemarchand S, Soria J, Legeais JM, Mirshahi M: **Expression of extracellular matrix proteins fibulin-1 and fibulin-2 by human corneal fibroblasts.** *Curr Eye Res* 2007, **32**:481–490.
32. Li L, Arman E, Ekblom P, Edgar D, Murray P, Lonai P: **Distinct GATA6- and laminin-dependent mechanisms regulate endodermal and ectodermal embryonic stem cell fates.** *Development* 2004, **131**:5277–5286.
33. Anderson C, Thorsteinsdottir S, Borycki AG: **Sonic hedgehog-dependent synthesis of laminin alpha1 controls basement membrane assembly in the myotome.** *Development* 2009, **136**:3495–3504.
34. Patton BL, Miner JH, Chiu AY, Sanes JR: **Distribution and function of laminins in the neuromuscular system of developing, adult, and mutant mice.** *J Cell Biol* 1997, **139**:1507–1521.
35. Visse R, Nagase H: **Matrix metalloproteinases and tissue inhibitors of metalloproteinases: structure, function, and biochemistry.** *Circ Res* 2003, **92**:827–839.
36. Neumann C, Yu A, Welge-Lussen U, Lutjen-Drecoll E, Birke M: **The effect of TGF-beta2 on elastin, type VI collagen, and components of the proteolytic degradation system in human optic nerve astrocytes.** *Invest Ophthalmol Vis Sci* 2008, **49**:1464–1472.
37. Richter B, Bandeira-Echtler E, Bergerhoff K, Lerch C: **Emerging role of dipeptidyl peptidase-4 inhibitors in the management of type 2 diabetes.** *Vasc Health Risk Manag* 2008, **4**:753–768.
38. Pala L, Rotella CM: **The role of DPP4 activity in cardiovascular districts: in vivo and in vitro evidence.** *J Diabetes Res* 2013, **2013**:590456.
39. Farid AS, Horii Y: **Modulation of paraoxonases during infectious diseases and its potential impact on atherosclerosis.** *Lipids Health Dis* 2012, **11**:92.
40. Meilin E, Aviram M, Hayek T: **Paraoxonase 2 (PON2) decreases high glucose-induced macrophage triglycerides (TG) accumulation, via inhibition of NADPH-oxidase and DGAT1 activity: studies in PON2-deficient mice.** *Atherosclerosis* 2010, **208**:390–395.
41. Botting R: **COX-1 and COX-3 inhibitors.** *Thromb Res* 2003, **110**:269–272.
42. Patrignani P, Tacconelli S, Sciulli MG, Capone ML: **New insights into COX-2 biology and inhibition.** *Brain Res Brain Res Rev* 2005, **48**:352–359.
43. Ghosh M, Tucker DE, Burchett SA, Leslie CC: **Properties of the Group IV phospholipase A2 family.** *Prog Lipid Res* 2006, **45**:487–510.
44. Pyagay P, Heroult M, Wang Q, Lehnert W, Belden J, Liaw L, Friesel RE, Lindner V: **Collagen triple helix repeat containing 1, a novel secreted protein in injured and diseased arteries, inhibits collagen expression and promotes cell migration.** *Circ Res* 2005, **96**:261–268.

45. McGrath JA, Uitto J: **The filaggrin story: novel insights into skin-barrier function and disease.** *Trends Mol Med* 2008, **14**:20–27.
46. Bouwstra JA, Ponec M: **The skin barrier in healthy and diseased state.** *Biochim Biophys Acta* 2006, **1758**:2080–2095.
47. Yamaguchi T, Osumi T: **Chanarin-Dorfman syndrome: deficiency in CGI-58, a lipid droplet-bound coactivator of lipase.** *Biochim Biophys Acta* 2009, **1791**:519–523.

doi:10.1186/1750-1172-8-197
Cite this article as: Hara *et al.*: Quantitative proteomic analysis of cultured skin fibroblast cells derived from patients with triglyceride deposit cardiomyovasculopathy. *Orphanet Journal of Rare Diseases* 2013 **8**:197.

Submit your next manuscript to BioMed Central and take full advantage of:

- Convenient online submission
- Thorough peer review
- No space constraints or color figure charges
- Immediate publication on acceptance
- Inclusion in PubMed, CAS, Scopus and Google Scholar
- Research which is freely available for redistribution

Submit your manuscript at
www.biomedcentral.com/submit

BioMed Central

A novel mechanism of keratin cytoskeleton organization through casein kinase Iα and FAM83H in colorectal cancer

Takahisa Kuga[1,*], Hideaki Kume[1], Naoko Kawasaki[1], Misako Sato[1], Jun Adachi[1], Takashi Shiromizu[1], Isamu Hoshino[2], Takanori Nishimori[2], Hisahiro Matsubara[2] and Takeshi Tomonaga[1,*]

[1]Laboratory of Proteome Research, National Institute of Biomedical Innovation, Ibaraki, Osakai 567-0085, Japan
[2]Department of Frontier Surgery, Graduate School of Medicine, Chiba University, Chuo-ku, Chiba 260-8670, Japan
*Authors for correspondence (t-kuga@nibio.go.jp; tomonaga@nibio.go.jp)

Accepted 9 July 2013
Journal of Cell Science 126, 4721–4731
© 2013. Published by The Company of Biologists Ltd
doi: 10.1242/jcs.129684

Summary

Keratin filaments form cytoskeletal networks in epithelial cells. Dynamic rearrangement of keratin filament networks is required for epithelial cells to perform cellular processes such as cell migration and polarization; however, the mechanism governing keratin filament rearrangement remains unclear. Here, we describe a novel mechanism of keratin cytoskeleton organization mediated by casein kinase Iα (CK-1α) and a newly identified keratin-associated protein, FAM83H. Knockdown of FAM83H induces keratin filament bundling, whereas overexpression of FAM83H disassembles keratin filaments, suggesting that FAM83H regulates the filamentous state of keratins. Intriguingly, keratin filament bundling is concomitant with the dissociation of CK-1α from keratin filaments, whereas aberrant speckle-like localization of CK-1α is observed concomitantly with keratin filament disassembly. Furthermore, CK-1α inhibition, similar to FAM83H knockdown, causes keratin filament bundling and reverses keratin filament disassembly induced by FAM83H overexpression, suggesting that CK-1α mediates FAM83H-dependent reorganization of keratin filaments. Because the N-terminal region of FAM83H interacts with CK-1α and the C-terminal region interacts with keratins, FAM83H might tether CK-1α to keratins. Colorectal cancer tissue also shows keratin filament disassembly accompanied with FAM83H overexpression and aberrant CK-1α localization, and FAM83H-overexpressing cancer cells exhibit loss or alteration of epithelial cell polarity. Importantly, knockdown of FAM83H inhibits cell migration accompanied by keratin cytoskeleton rearrangement in colorectal cancer cells. These results suggest that keratin cytoskeleton organization is regulated by FAM83H-mediated recruitment of CK-1α to keratins, and that keratin filament disassembly caused by overexpression of FAM83H and aberrant localization of CK-1α could contribute to the progression of colorectal cancer.

Key words: Keratin cytoskeleton, Casein kinase Iα, FAM83H, Colorectal cancer, Invasion

Introduction

Keratins are intermediate filament proteins that form cytoskeletal filament networks in epithelial cells (Moll et al., 2008; Oriolo et al., 2007; Windoffer et al., 2011). To form a filamentous structure, keratin proteins are nucleated, assembled into particles and then elongated (Miller et al., 1991; Miller et al., 1993; Windoffer et al., 2011). Keratin filaments are further bundled to form a mechanically stable cytoskeleton (Moll et al., 2008; Windoffer et al., 2011). Keratin filament assembly and bundling are dynamic and reversible processes (Flitney et al., 2009; Windoffer and Leube, 1999; Windoffer et al., 2004). The keratin cytoskeleton is an important structural stabilizer of epithelial cells (Moll et al., 2008). However, to achieve various dynamic cellular processes, including epithelial cell polarization and migration, keratin filament networks need to be dynamically reorganized (Ameen et al., 2001; Beil et al., 2003; Kölsch et al., 2010; Oriolo et al., 2007; Salas et al., 1997; Windoffer et al., 2011).

Although the molecular mechanism governing the rearrangement of keratin filaments is largely unclear, phosphorylation and protein–protein interactions of keratins have been shown to be involved (Izawa and Inagaki, 2006; Omary et al., 2006; Windoffer et al., 2011). Phosphorylation of keratins induces the disassembly of keratin filaments. Keratin filaments reconstituted using rat keratin 8 and keratin 18 were disassembled by *in vitro* phosphorylation of the keratins, but reassembled by their dephosphorylation (Yano et al., 1991). Upon treatment of epithelial cells with the protein phosphatase inhibitors okadaic acid and orthovanadate, phosphorylation levels of keratins were enhanced and keratin filaments were concomitantly disassembled (Strnad et al., 2001; Strnad et al., 2002); however, only a few kinases such as p38 MAPK and PKCζ were reported to be involved in keratin filament disassembly in different situations (Sivaramakrishnan et al., 2009; Wöll et al., 2007).

The bundling of keratin filaments seems to be regulated by the association of keratins with specific proteins (Windoffer et al., 2011). The plakin family proteins, which are linker proteins between keratin filaments and various cytoskeletal structures (Wiche, 1998), are major modulators of keratin filament bundling (Boczonadi et al., 2007; Liu et al., 2011; Long et al., 2006; Osmanagic-Myers et al., 2006); however, our knowledge about

Journal of Cell Science

crucial modulators of keratin filament bundling remains very limited. To further understand the mechanism governing the rearrangement of keratin filaments, identification of novel keratin-associated proteins and kinases responsible for the mechanism is required.

Similar to normal epithelial cells, epithelial cancer cells also express keratin proteins (Moll et al., 2008; Omary et al., 2009). Several studies have reported the involvement of keratins in cancer progression, invasion and metastasis (Omary et al., 2009). In several types of cancer, the expression levels of specific subtypes of keratin correlate with patient survival (Moll et al., 2008). In colorectal cancer, reduced expression of keratin 8 and keratin 20 was associated with shorter patient survival (Knösel et al., 2006). Furthermore, several reports have suggested a direct beneficial impact of keratins in cancer treatment. Forced expression of keratin 18 in MDA-MB-231 breast cancer cells strengthened cell–cell adhesions and markedly regressed tumor growth and metastasis in a xenograft model (Bühler and Schaller, 2005). Pancreatic carcinoma cells also exhibited decreased motility and tumorigenicity upon forced expression of keratin 18 (Pankov et al., 1997); however, additional studies are needed to elucidate the role of keratins in cancer.

FAM83H is an essential protein for amelogenesis because its truncated mutations cause autosomal-dominant hypocalcified amelogenesis imperfecta (Kim et al., 2008; Urzúa et al., 2011). However, very recent reports suggest the involvement of FAM83H in cancer. Microarray analysis of cancer tissues indicate increased expression of FAM83H in various types of cancer, including colorectal cancer (Sasaroli et al., 2011). Furthermore, Hatanaka and colleagues performed a focus formation assay using the cDNA library prepared from biliary tract cancer tissue and showed that fragmented FAM83H cDNA possesses transforming activity (Hatanaka et al., 2010). In a phospho-proteomic study of lung cancer cell lines that are sensitive or resistant to the anticancer drug dasatinib, phosphorylation levels of FAM83H decreased approximately tenfold in dasatinib-resistant cell lines (Klammer et al., 2012), implying the involvement of FAM83H in the resistance to dasatinib; however, there have been no reports on the precise mechanisms.

In this study, we determined that FAM83H and casein kinase Iα (CK-1α) are novel keratin-associated proteins and demonstrate that FAM83H-mediated recruitment of CK-1α to keratin filaments controls the filamentous state of keratins in colorectal cancer cells. Furthermore, we show that overexpression of FAM83H and CK-1α-mediated disassembly of keratin filaments occur in colorectal cancer tissue. FAM83H-overexpressing cancer cells exhibit loss or alteration of epithelial cell polarity and cell–cell adhesions – a hallmark of highly motile cancer cells. Given that FAM83H is involved in reorganization of the keratin cytoskeleton during the migration of colorectal cancer cells, keratin filament disassembly induced by FAM83H overexpression and aberrant localization of CK-1α might be important for the migration and invasion of colorectal cancer.

Results

Associations of FAM83H and CK-1α with keratins

We first searched for proteins associated with FAM83H using a proteomic approach. HCT116 colorectal cancer cells were transfected with a plasmid vector encoding FLAG-tagged FAM83H or the empty vector, and immunoprecipitation with anti-FLAG antibody was performed using extracts of these cells. Proteins present in the immunoprecipitates were identified using in-gel digestion and LC-MS/MS. By comparing the proteins identified from FAM83H-FLAG immunoprecipitates with those from the control, keratin proteins (subtypes 18 and 19) and CK-1α were identified as FAM83H-associated proteins (supplementary material Table S1).

Western blot analysis of these immunoprecipitates substantiated the association of FAM83H with CK-1α and keratin 8 and 18 (Fig. 1A). Furthermore, endogenous FAM83H and CK-1α were detected in immunoprecipitates using anti-keratin-18 antibody

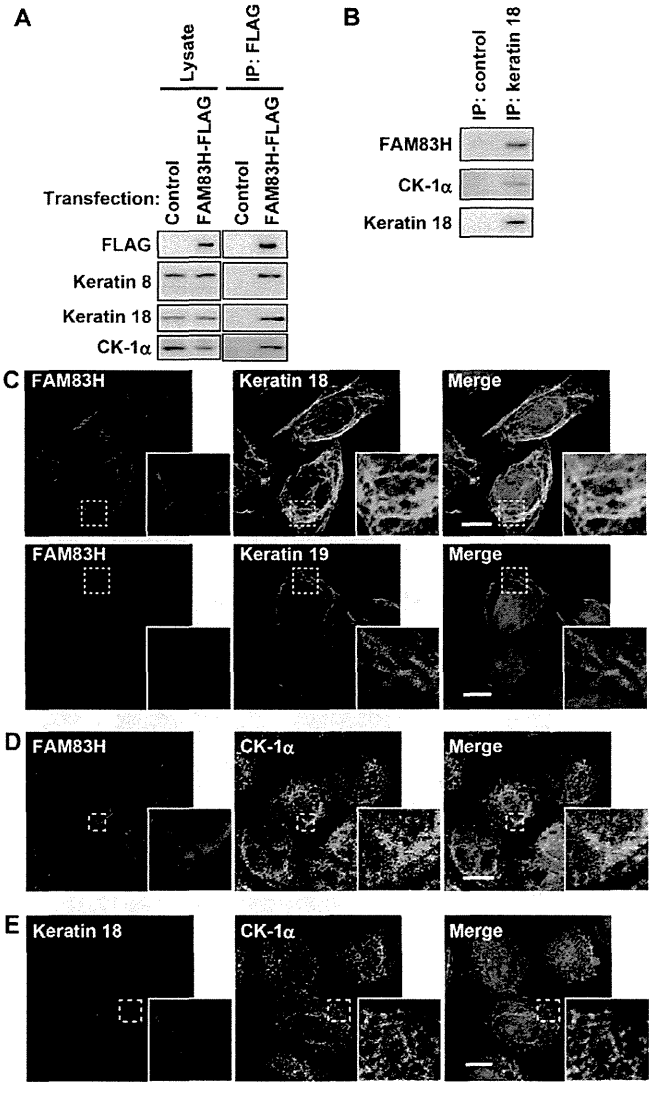

Fig. 1. Association of FAM83H and CK-1α with keratins.
(A) Immunoprecipitation with anti-FLAG antibody was performed using cell lysates from HCT116 cells treated with FAM83H–FLAG vector or the empty vector (control) for 24 hours. The cell lysates and immunoprecipitates were analyzed by western blotting. (B) Immunoprecipitates with anti-keratin-18 or the control antibody (MPOC-21) from DLD-1 cell lysates were analyzed by western blotting. (C–E) DLD1 cells were stained with the indicated antibodies. Small panels show magnified images of the areas enclosed by dotted lines. DNA is stained with DAPI (blue). Scale bars: 10 μm.

(Fig. 1B). Fig. 1C shows subcellular colocalization of FAM83H with keratin 18 and keratin 19, and Fig. 1D,E show partial colocalization of CK-1α with FAM83H and keratin 18 [Pearson's correlation coefficient: FAM83H vs keratin 18, $r=0.58\pm0.20$ ($n=6$ cell images); FAM83H vs keratin 19, $r=0.49\pm0.06$ ($n=6$ cell images); FAM83H vs CK-1α, $r=0.35\pm0.06$ ($n=11$ cell images); keratin 18 vs CK-1α, $r=0.31\pm0.07$ ($n=11$ cell images)]. Given that organization of the keratin cytoskeleton is regulated by protein phosphorylation (Omary et al., 2006), these results suggest that FAM83H and CK-1α is involved in keratin cytoskeleton organization.

FAM83H regulates the filamentous state of keratins

To assess whether FAM83H regulates the organization of keratin filaments, HCT116 cells were treated with siRNA to knock down FAM83H and keratin filaments were visualized. Control cells formed an intricate network of thin keratin filaments in the cytoplasm (Fig. 2A). In sharp contrast, FAM83H-knockdown cells constructed a markedly rough network of thick keratin filaments (Fig. 2A). Next, we tested the effect of overexpression of FAM83H–FLAG on keratin filaments in HCT116 cells. Fig. 2B shows that FAM83H–FLAG overexpression completely disassembled keratin filaments (region 1), although adjacent cells without FAM83H–FLAG expression exhibited normal networks of keratin filaments (region 2). FAM83H–FLAG mainly colocalized with the disassembled keratin proteins (Pearson's correlation coefficient, $r=0.78\pm0.20$ ($n=3$ cell images); Fig. 2B, region 1). In DLD1 colorectal cancer cells, similar reorganization of keratin filaments by knockdown and overexpression of FAM83H was observed (supplementary material Fig. S1).

In addition, western blot analysis showed that these alterations of the keratin filament networks were not due to changes in the expression levels of keratin proteins because no changes in the expression of keratin 8, keratin 18 or keratin 19 were observed upon knockdown or overexpression of FAM83H (Fig. 2A,B). Given that keratin filaments are dynamic cytoskeletal elements capable of rapid and reversible restructuring (Windoffer et al., 2011), these results indicate that FAM83H controls the equilibrium between the assembly (bundling) and disassembly of keratin filaments.

CK-1α mediates FAM83H-dependent rearrangement of keratin filaments

Next, we examined whether CK-1α is involved in the organization of keratin filaments. HCT116 cells were treated with a CK-1 inhibitor, D4476, or with siRNA to knock down CK-1α (CK-1α siRNA) and analyzed by immunofluorescence for keratin filaments. Inhibition of CK-1α, similar to FAM83H knockdown, promoted bundling of keratin filaments without changes in the protein level of keratins (Fig. 3A,B), implying that FAM83H and CK-1α cooperate to regulate the filamentous state of keratins. On the basis of the amino acid sequence, FAM83H does not have any enzymatic domains; thus, CK-1α kinase activity could mediate the mechanism by which FAM83H rearranges keratin filaments.

To explore the requirement of CK-1α for FAM83H rearrangement of keratin filaments, HCT116 cells were transfected with FAM83H–FLAG in the presence of CK-1α siRNA or D4476. Immunofluorescence for keratin filaments showed that both CK-1α siRNA and D4476 obviously reversed

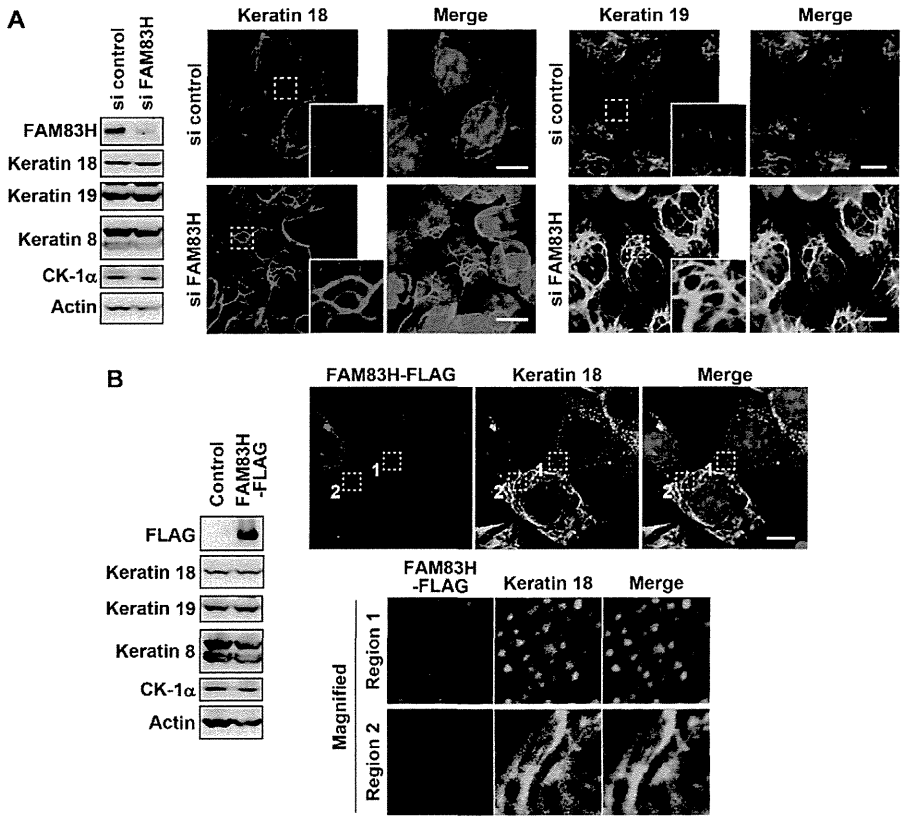

Fig. 2. Effects of knockdown and overexpression of FAM83H on the filamentous state of keratins. (A) HCT116 cells were treated with FAM83H siRNA or control siRNA for 2 days and analyzed by immunofluorescence and western blotting. Small panels show magnified images of the areas enclosed by dotted lines. (B) HCT116 cells were transfected with FAM83H–FLAG vector or the empty vector (control) and cultured for 24 hours. Western blotting and immunofluorescence were performed. Magnified images of the areas enclosed by dotted lines in cells with (region 1) and without (region 2) FAM83H–FLAG expression are shown. DNA is stained with DAPI (blue). Scale bars: 10 μm.

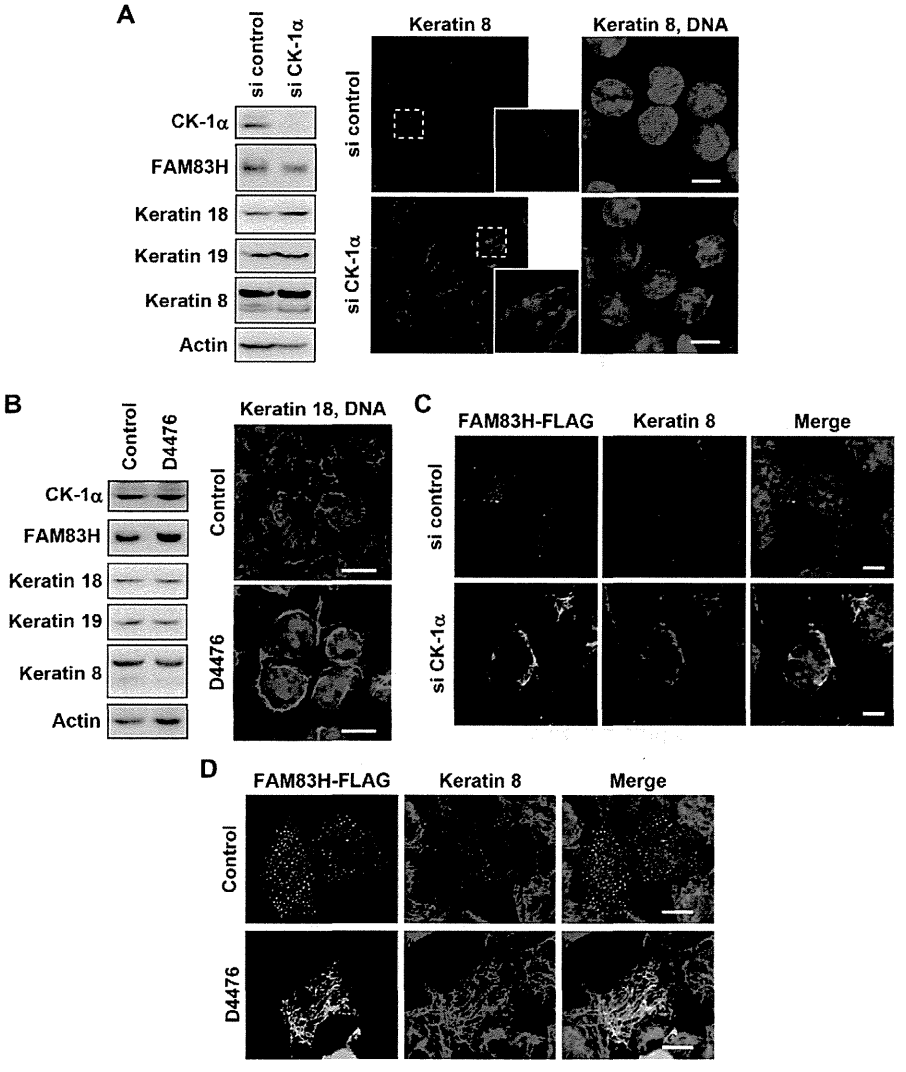

Fig. 3. CK-1α mediates FAM83H-dependent rearrangement of keratin filaments. (A) HCT116 cells were treated with CK-1α siRNA or control siRNA for 2 days and analyzed by immunofluorescence and western blotting. Insets show magnified images in the regions enclosed by dotted lines. (B) HCT116 cells were treated with D4476, a CK-1 inhibitor or DMSO (control) for 3 hours and analyzed by immunofluorescence and western blotting. Keratin 18 staining is shown in red. (C) HCT116 cells were transfected with CK-1α siRNA or control siRNA, followed by transfection of FAM83H–FLAG after 24 hours, and then cultured for 24 hours. Cells were analyzed by immunofluorescence. (D) HCT116 cells were transfected with FAM83H-FLAG and cultured for 24 hours. D4476 or DMSO (control) was added for the last 18 hours of the 24 hours culture. Cells were analyzed by immunofluorescence. DNA is stained with DAPI (blue). Scale bars: 10 μm.

the effect of FAM83H–FLAG on the disassembly of keratin filaments (Fig. 3C,D). These results suggest that CK-1α mediates FAM83H–dependent rearrangement of keratin filaments.

Keratin proteins have been subjected to phosphorylation to regulate their own structural state (Omary et al., 2006); however, we could not simply explain the mechanism of FAM83H- and CK-1α-mediated rearrangement of keratin filaments by phosphorylation, at least at Ser73 and Ser431 of keratin 8 and Ser33 and Ser52 of keratin 18 (see supplementary material Fig. S2).

FAM83H recruits CK-1α to keratin filaments

What is the precise mechanism by which FAM83H modulates the CK-1α-mediated rearrangement of keratin filaments? It is known that CK-1α is basically constitutive active and its subcellular localization is an important factor in its functional regulation (Knippschild et al., 2005); thus, FAM83H might regulate the subcellular localization of CK-1α. To test this hypothesis, we examined the effect of knockdown or overexpression of FAM83H on the subcellular localization of CK-1α. Immunofluorescence for CK-1α showed that FAM83H knockdown diminished the colocalization of CK-1α with keratin filaments (Fig. 4A). FAM83H knockdown decreased the value of the Pearson's correlation coefficient between CK-1α and keratin filaments (Fig. 4A). Conversely, FAM83H overexpression recruited CK-1α to disassembled keratin speckles (Fig. 4B). In FAM83H-overexpressing cells, CK-1α showed high values of the Pearson's correlation coefficient with FAM83H [$r=0.78\pm0.20$ ($n=3$ cell images)] and keratin 18 [$r=0.62\pm0.10$ ($n=6$ cell images)]. Coimmunoprecipitation assays using anti-keratin 18 antibody further showed that FAM83H knockdown abolished the physical interaction of CK-1α with keratin 18 (Fig. 4C). Neither knockdown nor inhibition of CK-1α affected the localization of FAM83H to keratins (Fig. 3C,D), excluding the possibility that CK-1α recruits FAM83H to keratins. These results indicate that FAM83H recruits CK-1α to keratin filaments to enable CK-1α to modulate the filamentous state of keratins.

FAM83H is a linker protein between CK-1α and keratins

To further elucidate the mechanism governing FAM83H-dependent rearrangement of keratin filaments, we performed proteomic analysis using dominant-negative truncated proteins of FAM83H (Lee et al., 2008; Urzúa et al., 2011; Wright et al.,

Journal of Cell Science

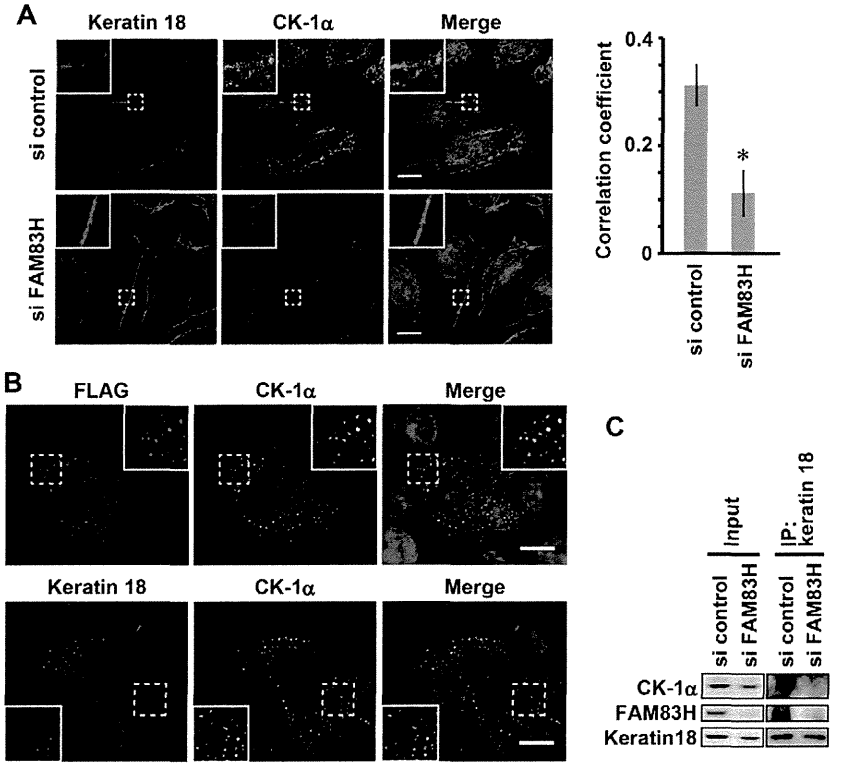

Fig. 4. FAM83H recruits CK-1α to keratin filaments. (A) DLD1 cells were transfected with FAM83H siRNA or control siRNA for 2 days and analyzed by immunofluorescence. Colocalization of CK-1α and keratin 18 was evaluated by the Pearson's correlation coefficient. Quantification data are presented as the mean ± s.d. calculated from at least ten cell images. Asterisk indicates a significant difference from the control (two-tailed Student's *t*-test, $*P<0.0001$). (B) HCT116 cells were transfected with FAM83H–FLAG for 24 hours and analyzed by immunofluorescence. DNA is stained with DAPI (blue). Insets show magnified images in the regions enclosed by dotted lines (A,B). Scale bars: 10 μm (A,B). (C) DLD1 cells transfected with FAM83H siRNA or control siRNA for 2 days were analyzed by coimmunoprecipitation assay using anti-keratin-18 antibody. Immunoprecipitates were examined by western blotting.

2009). Similar to FAM83H knockdown, transfection with a plasmid encoding FAM83H-truncated protein with a FLAG-tag [amino acids 1–286, FAM83H-286N–FLAG; 1–296, FAM83H-296N–FLAG] induced the aggregation of severely bundled keratin filaments in HCT116 cells (Fig. 5A and data not shown). LC-MS/MS analysis of coimmunoprecipitated proteins with FAM83H-286N–FLAG and FAM83H–FLAG (full-length) showed that FAM83H-286N–FLAG immunoprecipitates contained higher levels of CK-1α but lower levels of keratins than FAM83H–FLAG immunoprecipitates (supplementary material Table S2). Western blotting of these immunoprecipitates substantiated strong interactions of FAM83H-286N–FLAG with CK-1α but only marginal interaction with keratin 8 (Fig. 5B). These analyses suggest that FAM83H interacts with CK-1α in the N-terminal region and with keratins at the C-terminal region. Additionally, forced expression of FAM83H-286N–FLAG diminished the recruitment of CK-1α to keratin filaments (Fig. 5C). FAM83H-286N–FLAG significantly decreased the value of the Pearson's correlation coefficient between CK-1α and keratin filaments (Fig. 5C). FAM83H-286N–FLAG appeared to exert a dominant-negative effect on the recruitment of CK-1α to keratins. These results suggest that FAM83H tethers CK-1α to keratins and that a FAM83H-mediated interaction between CK-1α and keratins is needed for proper keratin cytoskeleton organization.

A CK-1α binding motif of FAM83H

FAM83H has FxxxF amino acid sequences (x, any amino acid residue), known to be CK-1-binding motifs of NFAT1, PER1 and PER2 (Okamura et al., 2004), in the N-terminal region (FMWSF, 247–251 aa; FDEEFRILF, 270–278 aa). To assess the requirement of these amino acid sequences for the binding of FAM83H to CK-1α, a coimmunoprecipitation assay using alanine mutants of FAM83H (251A, FMWSA; 274A, FDEEARILF) was performed. The FLAG-tagged FAM83H alanine mutants were transfected into HCT116 cells and immunoprecipitated using anti-FLAG antibody. Compared with wild-type FAM83H and the 251A mutant, immunoprecipitates of the 274A mutant contained very low levels of CK-1α (Fig. 6A), suggesting that the FDEEFRILF sequence is the major motif of FAM83H for CK-1α binding.

We further tested whether the 274A mutation disabled the FAM83H function to control keratin filament organization. HCT116 cells were transfected with FAM83H-274A or FAM83H-251A and analyzed by immunofluorescence of keratin filaments. Overexpression of the 251A mutant, as well as wild-type FAM83H, caused disassembly of keratin filaments, whereas the 274A mutant did not affect keratin filament organization (Fig. 6B). In addition, speckle-like localization of CK-1α was not induced by overexpression of FAM83H-274A, in contrast to wild-type FAM83H or FAM83H-251A (Fig. 6C). Taken together, these results substantiate that interaction of FAM83H with CK-1α is required for keratin filament reorganization.

Disassembly of keratin filaments by overexpression of FAM83H in human colorectal cancer tissue

To examine the expression of FAM83H in colorectal cancer cells *in vivo*, colorectal cancer tissues were analyzed by quantitative PCR (qPCR) and immunostaining with anti-FAM83H antibody. *FAM83H* mRNA levels were elevated in 10 of 12 colorectal cancer tissues compared with adjacent non-tumor tissues (Fig. 7A). Increased expression of FAM83H protein was also observed in 75 of 111 specimens, as assessed by the intensity of FAM83H immunostaining in cancer cells and adjacent normal

Journal of Cell Science

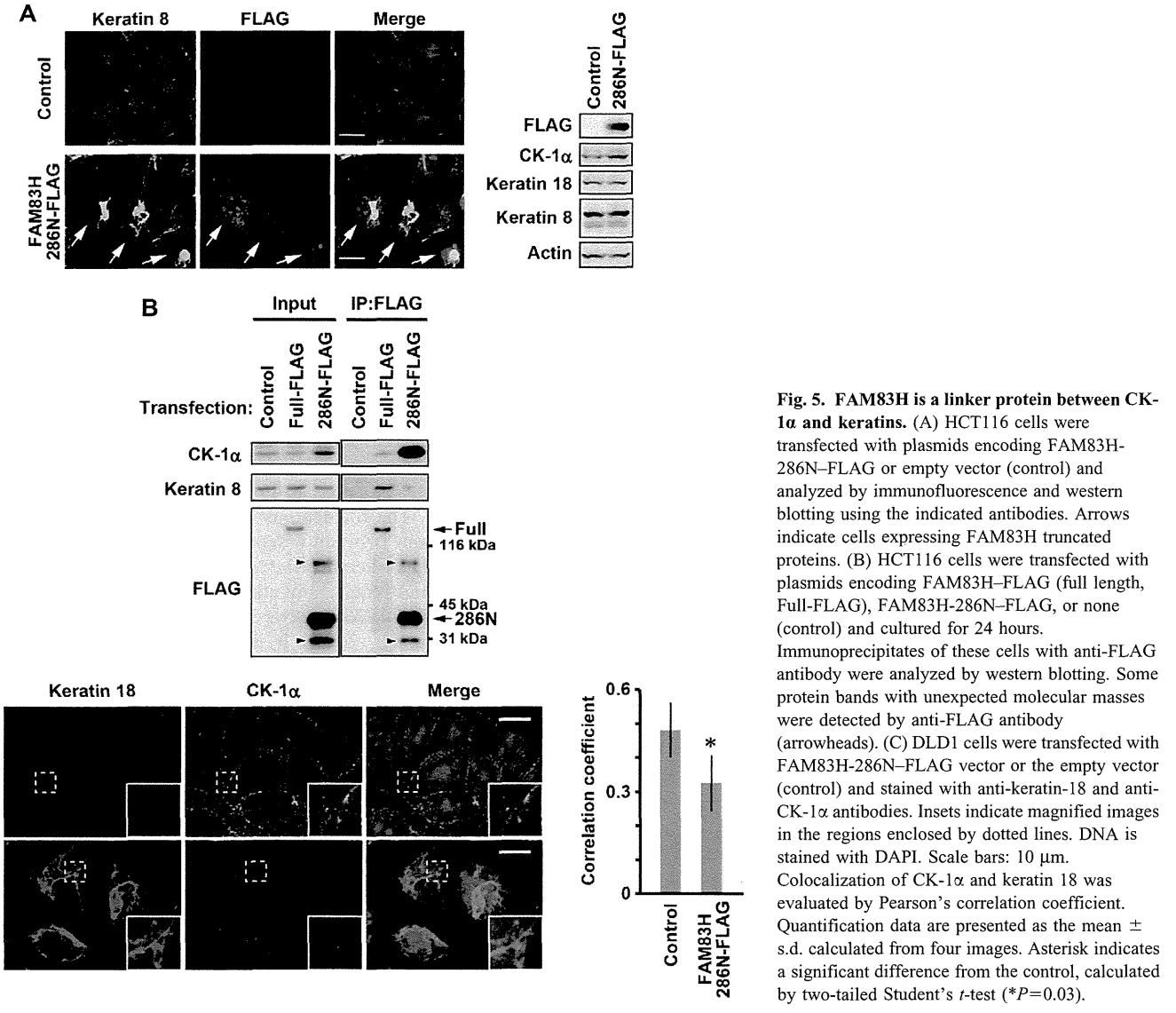

Fig. 5. FAM83H is a linker protein between CK-1α and keratins. (A) HCT116 cells were transfected with plasmids encoding FAM83H-286N–FLAG or empty vector (control) and analyzed by immunofluorescence and western blotting using the indicated antibodies. Arrows indicate cells expressing FAM83H truncated proteins. (B) HCT116 cells were transfected with plasmids encoding FAM83H–FLAG (full length, Full-FLAG), FAM83H-286N–FLAG, or none (control) and cultured for 24 hours. Immunoprecipitates of these cells with anti-FLAG antibody were analyzed by western blotting. Some protein bands with unexpected molecular masses were detected by anti-FLAG antibody (arrowheads). (C) DLD1 cells were transfected with FAM83H-286N–FLAG vector or the empty vector (control) and stained with anti-keratin-18 and anti-CK-1α antibodies. Insets indicate magnified images in the regions enclosed by dotted lines. DNA is stained with DAPI. Scale bars: 10 μm. Colocalization of CK-1α and keratin 18 was evaluated by Pearson's correlation coefficient. Quantification data are presented as the mean ± s.d. calculated from four images. Asterisk indicates a significant difference from the control, calculated by two-tailed Student's *t*-test (**P*=0.03).

epithelial cells (Fig. 7B). Note that the FAM83H expression pattern was heterogeneous throughout the tumor mass (Fig. 7C) and a subpopulation of cancer cells exhibited markedly high levels of FAM83H expression (Fig. 7C, region 1). Consistent with the *in vitro* results, FAM83H-overexpressing cancer cells exhibited disassembled keratin filaments and aberrant speckle-like colocalization of FAM83H, CK-1α and disassembled keratins (Fig. 7D,E). Another important feature of FAM83H-overexpressing cancer cells was loss or alteration of epithelial cell polarity (apical-basal polarity) (Fig. 7C, region 1) compared with FAM83H-low cancer cells (Fig. 7C, region 2). In addition, loss of E-cadherin expression, a protein that is essential for cell–cell adhesion (Birchmeier and Behrens, 1994), was also detected in FAM83H-overexpressing cancer cells (Fig. 7F). Given that the loss of epithelial cell polarity and E-cadherin expression is known to be a process during the migration or invasion of cancer cells (Thiery et al., 2009), these *in vivo* data suggest that FAM83H overexpression and the subsequent disassembly of keratin filaments occur in migrating or invading cancer cells.

FAM83H is involved in reorganization of the keratin cytoskeleton during migration of colorectal cancer cells

Reorganization of the keratin cytoskeleton is required for the migration of epithelial cells (Beil et al., 2003; Kölsch et al., 2010; Windoffer et al., 2011). To examine whether FAM83H was involved in the migration of colorectal cancer cells, we performed a wound-healing assay with FAM83H-knockdown cells. HCT116 cells treated with FAM83H siRNA or control siRNA were scratched, and the wound edge was monitored by microscopy. Treatment with FAM83H siRNA suppressed migration of the wound edge of the cell sheets to less than 50% (Fig. 8A). Visualization of the cells at the wound edge using anti-α-tubulin and anti-keratin-8 antibodies showed that control cells formed a cell-spreading structure at the wound edge and showed a redistribution of keratin filaments that was less abundant in the cell-spreading region compared with the cell body region (Fig. 8B). By contrast, FAM83H-knockdown cells formed severely bundled keratin filaments throughout the cytoplasm and were prevented from spreading outward at the wound edge

Journal of Cell Science

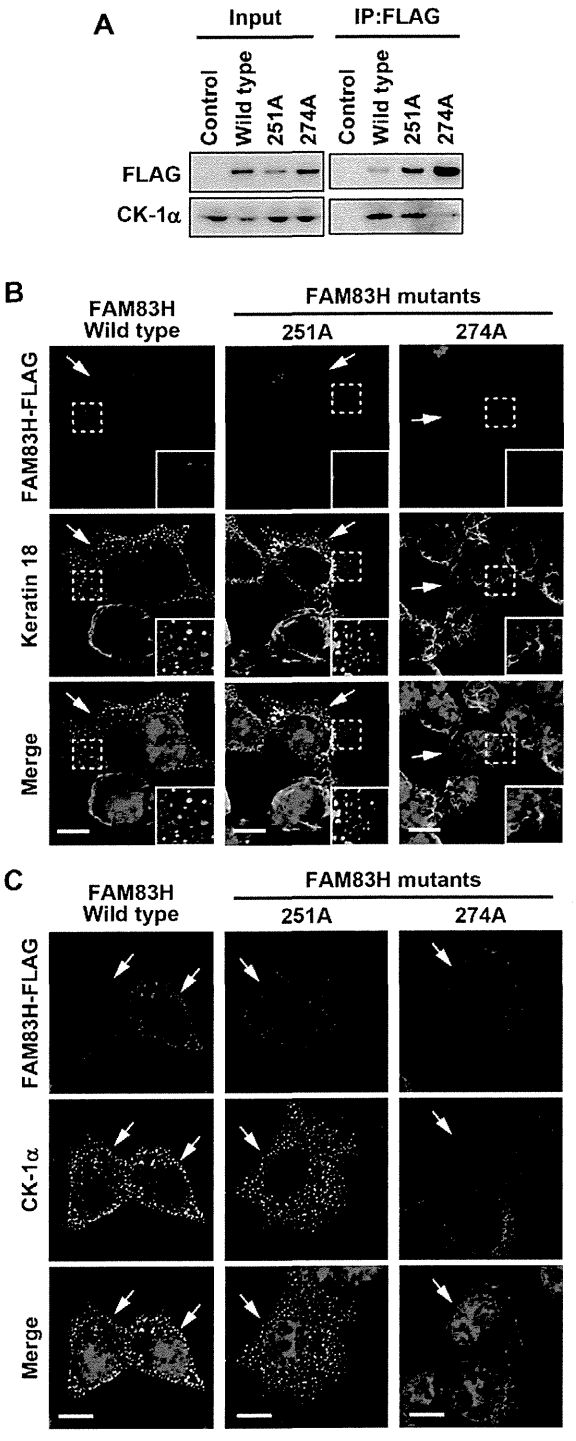

Fig. 6. A CK-1α-binding motif of FAM83H. (A) Immunoprecipitation with anti-FLAG antibody was performed using lysates from HCT116 cells transfected with wild-type FAM83H–FLAG, FAM83H-251A–FLAG or FAM83H-274A–FLAG. Input lysates and immunoprecipitates were analyzed by western blotting. (B,C) HCT116 cells were transfected with wild-type FAM83H–FLAG, FAM83H-251A–FLAG or FAM83H-274A–FLAG and analyzed by immunofluorescence with the indicated antibodies. DNA is stained with DAPI (blue). Arrows indicate cells expressing FLAG-tagged proteins. Insets indicate magnified images in the areas enclosed by dotted lines. Scale bars: 10 μm.

(Fig. 8B). These results suggest that FAM83H plays a crucial role in cell migration by regulating keratin cytoskeleton organization.

Discussion

In this study, we identified novel keratin-associated proteins, FAM83H and CK-1α, and demonstrated that FAM83H regulates keratin cytoskeleton organization by recruiting CK-1α to keratin filaments, both *in vitro* and *in vivo*. Moreover, loss of epithelial cell polarity and E-cadherin expression, in addition to keratin filament disassembly, was observed in FAM83H-overexpressing cancer cells *in vivo*. These results strongly suggest that CK-1α-mediated keratin filament disassembly induced by FAM83H overexpression is involved in the invasion and/or metastasis of colorectal cancer.

Although it has been undoubtedly accepted that the filamentous state of keratins is regulated by protein phosphorylation (Izawa and Inagaki, 2006; Omary et al., 2006; Windoffer et al., 2011), little is known about the kinases responsible for the rearrangement of keratin filaments; thus, our data showing the role of CK-1α in keratin filament rearrangement are valuable. The filamentous state of keratins is modulated by the equilibrium between assembly (bundling) and disassembly. The assembly of keratin filaments is a self-processing reaction, which does not require any additional proteins, at least *in vitro* (Steinert et al., 1976), and is highly favored over disassembly (Windoffer et al., 2011). It is therefore conceivable that the mechanism governing the disassembly of keratin filaments plays a crucial role in regulating the equilibrium of filamentous states of keratins. Aberrant speckle-like colocalization of CK-1α to keratin filaments causes disassembly of keratin filaments, whereas dissociation of CK-1α from keratin filaments causes bundling of keratin filaments. These results suggest that correct recruitment of CK-1α to keratin filaments is required to properly maintain the equilibrium of the filamentous state of keratins.

Because CK-1α-mediated disassembly of keratin filaments depends on the kinase activity of CK-1α (Fig. 3B,D), identification of the CK-1α substrates responsible for keratin filament disassembly is an important issue. As keratin proteins are known to be subject to phosphorylation to regulate their own filament status (Omary et al., 2006), keratin proteins themselves are major candidates of the CK-1α substrates; however, we could not explain the CK-1α-mediated reorganization of keratin filaments by phosphorylation, at least at Ser73 and Ser431 of keratin 8 and Ser33 and Ser52 of keratin 18 (supplementary material Fig. S2). Another candidate for CK-1α substrates is plectin, which plays a crucial role in crosslinking keratin filaments to other cellular structures (Wiche, 1998). FAM83H–FLAG immunoprecipitates contained plectin (supplementary material Table S1), and plectin knockdown, as well as the inhibition of FAM83H and CK-1α, caused keratin filament bundling in HCT116 cells (supplementary material Fig. S3) and a human liver cell line (Liu et al., 2011). Our next task will be proteomic analysis to identify the CK-1α substrates responsible for the rearrangement of keratin filaments.

CK-1α is basically constitutive active and thus its subcellular distribution is an important factor for functional regulation (Knippschild et al., 2005); however, the precise mechanism governing the subcellular distribution of CK-1α remains largely unknown. We determined that FAM83H is a novel key regulator of the subcellular distribution of CK-1α. FAM83H was found to be a linker protein between CK-1α and keratins, because

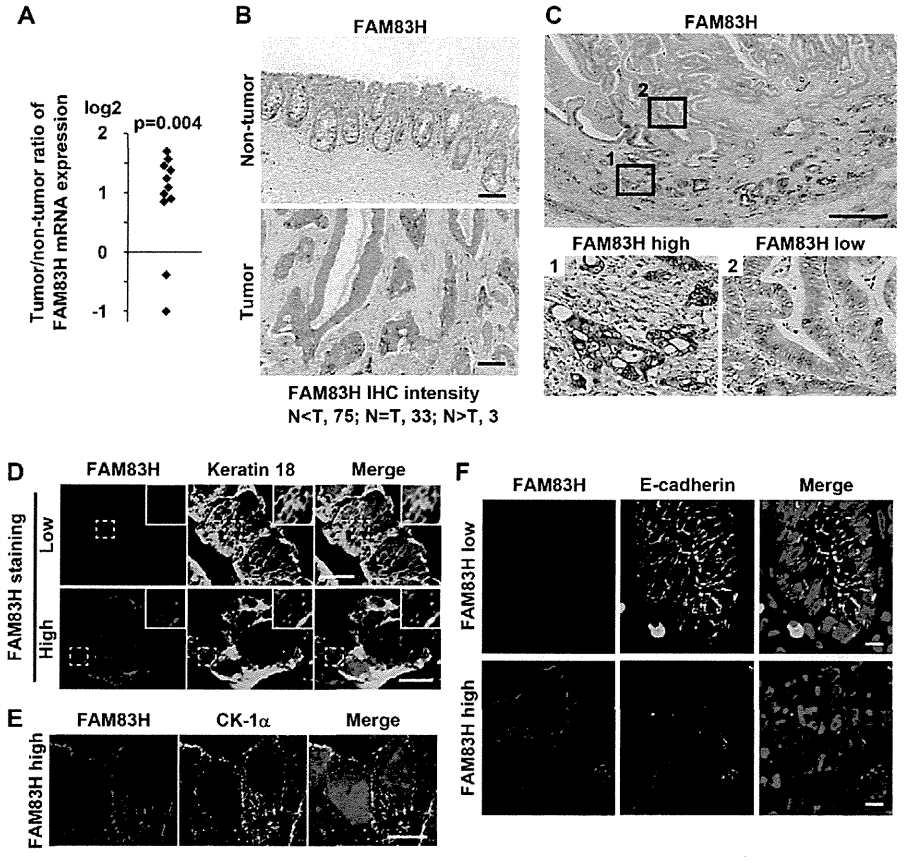

Fig. 7. Disassembly of keratin filaments and loss of epithelial cell polarity in FAM83H-overexpressing human colorectal cancer tissue. (A) Tumor and the adjacent non-tumor tissues from 12 colorectal cancer patients were analyzed by qPCR. The expression level of FAM83H in each tumor sample was normalized by that in the corresponding non-tumor sample. The values are expressed as log2 ratios. Significant differences between tumor and non-tumor samples were calculated by double-tailed Student's paired *t*-test ($P=0.004$). (B,C) Paraffin-embedded cancer tissue specimens from 111 different patients were stained with anti-FAM83H antibody. Staining intensity for FAM83H in cancer cells was high in 75 specimens, similar in 33 specimens or low in 3 specimens, compared with that in adjacent non-tumor epithelial cells. The boxed regions (regions 1 and 2) are magnified below (C). (D–F) Immunofluorescence of snap-frozen cancer tissues using the indicated antibodies. Images of cancer cells expressing high or low levels of FAM83H are shown. Insets indicate magnified images in the regions enclosed by dotted lines. DNA was stained with DAPI (blue). Scale bars: 100 μm (B); 1 mm (C); 10 μm (D–F).

FAM83H interacts with CK-1α in the N-terminal region and keratins in the C-terminal region. Consistent with the cases of NFAT1, PER1 and PER2 (Okamura et al., 2004), FAM83H interacts with CK-1α through an FxxxF amino acid sequence in the N-terminal region (FDEEFRILF, 270–278 aa).

Intriguingly, FAM83H overexpression not only induced aberrant recruitment of CK-1α to keratin filaments but also decreased cytoplasmic localization of CK-1α (Fig. 4). Cytoplasmic CK-1α plays an essential role in the phosphorylation and degradation of β-catenin (Knippschild et al., 2005). Loss of CK-1α-mediated phosphorylation of β-catenin causes nuclear accumulation of β-catenin and transcription of Wnt-specific genes responsible for the control of cell fate decisions, resulting in tumorigenesis (Elyada et al., 2011; Polakis, 2000; Valenta et al., 2012). In fact, we observed dephosphorylation and nuclear accumulation of β-catenin upon FAM83H overexpression *in vitro* and *in vivo* (unpublished data). These results suggest that the subcellular distribution and function of CK-1α are totally orchestrated by FAM83H expression levels.

Our *in vivo* data suggested the physiological significance of the mechanism governing the rearrangement of keratin filaments by FAM83H and CK-1α in colorectal cancer. FAM83H overexpression, aberrant localization of CK-1α, and keratin filament disassembly are all detected in colorectal cancer cells exhibiting loss or alteration of epithelial cell polarity. As discussed above, CK-1α is involved in Wnt–β-catenin signaling, which regulates the epithelial cell polarity of cancer cells (Thiery et al., 2009); thus, the aberrant localization of CK-1α might contribute to the loss of epithelial cell polarity. In addition, because the keratin cytoskeleton is an essential element for maintenance of epithelial cell polarity (Ameen et al., 2001; Oriolo et al., 2007; Salas et al., 1997), keratin filament disassembly caused by FAM83H overexpression may also occur during the loss of epithelial cell polarity.

E-cadherin expression is also suppressed in FAM83H-overexpressing cancer cells *in vivo*. Loss of E-cadherin expression, as well as that of epithelial cell polarity, is a hallmark of epithelial–mesenchymal transition (EMT), which is a process by which cancer cells escape from the primary tumor mass for invasion and metastasis (Thiery et al., 2009). Moreover, E-cadherin expression is controlled by Wnt/β-catenin signaling (Thiery et al., 2009). These results imply that the aberrant localization of CK-1α caused by FAM83H overexpression might be involved in the suppression of E-cadherin and EMT of colorectal cancer cells.

Several reports have suggested that expression levels of keratin proteins are correlated to the cancer grade and patient survival (Knösel et al., 2006; Moll et al., 2008) and that keratin 18 contributes to suppression of the invasiveness of breast and pancreatic cancer cells (Bühler and Schaller, 2005; Pankov et al., 1997). In addition, Beil and colleagues proposed that reorganization of the keratin cytoskeleton by sphingosylphosphorylcholine induced cellular elasticity and enhanced cell migration of pancreatic cancer cells (Beil et al., 2003). Given our *in vitro* data suggesting the role of FAM83H-mediated rearrangement of keratin filaments in the migration of colorectal cancer cells, these results suggest that the disassembly of keratin filaments by overexpression of FAM83H contributes to the invasion and metastasis of colorectal cancer.

Journal of Cell Science

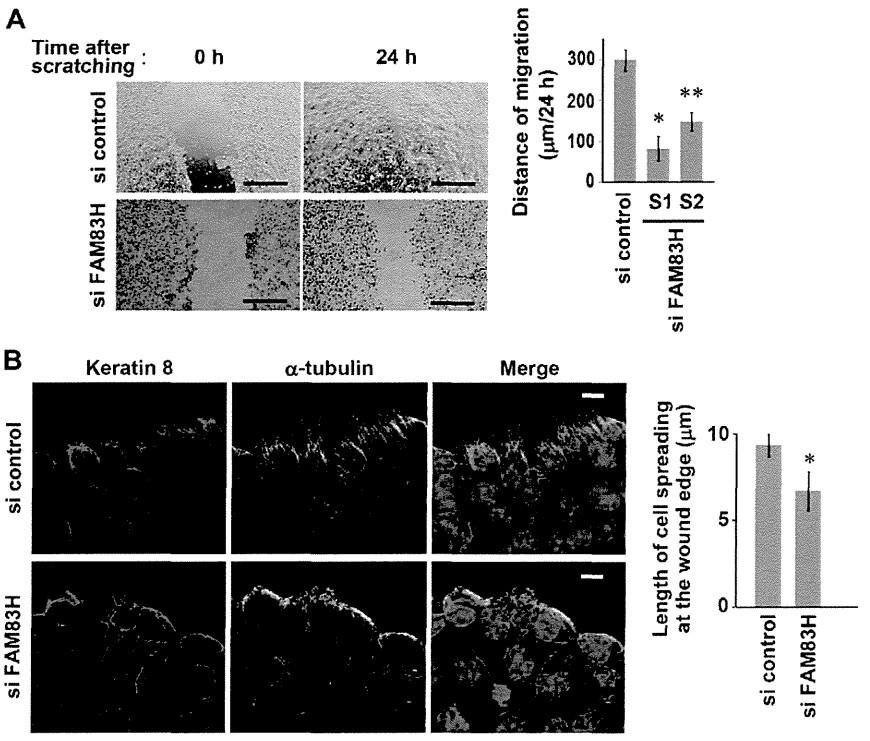

Fig. 8. FAM83H knockdown inhibits reorganization of the keratin cytoskeleton during migration of colorectal cancer cells. (A) HCT116 cells were treated with FAM83H siRNA or control siRNA for 24 hours, and then the cell sheets were scratched and cultured for 24 hours. Representative images of the cell sheets at 0 and 24 hours after scratching are shown. The migration distance of the wound edge of the cell sheets during 24 hours of culture was measured. Quantification data are presented as the mean ± s.d. of three experiments. (B) HCT116 cells were treated with FAM83H siRNA or control siRNA for 36 hours and the cell sheets were scratched. The cells were then cultured for 6 hours and stained with anti-keratin-8 and anti-α-tubulin antibodies, and DAPI (blue). Confocal images of representative cells at the wound edge are shown. The extent of spread of each leading cell at the wound edge was assessed by measuring the distance from the nucleus to the cell periphery. Quantification data are presented as the mean ± s.d. of three experiments. Approximately 100 leading cells were assessed in each experiment. Asterisks indicate significant differences from the control, calculated by two-tailed Student's *t*-test (**P*=0.0007, ***P*=0.001 in A; **P*=0.02 in B). Scale bars: 500 μm (A); 10 μm (B).

In conclusion, this work elucidated a novel mechanism governing the rearrangement of keratin filaments in colorectal cancer cells. Our data also suggested that aberrant localization of CK-1α and keratin filament disassembly induced by FAM83H overexpression are involved in the migration of colorectal cancer cells. FAM83H overexpression was suggested in various types of cancer (Sasaroli et al., 2011), and CK-1α is known to play a tumor suppressive role (Elyada et al., 2011; Valenta et al., 2012). Thus, tumor progression of various types of cancer might be commonly promoted by FAM83H overexpression, malfunction of CK-1α and subsequent disassembly of keratin filaments.

Materials and Methods

Cell culture and transfection

HCT116 and DLD1 colorectal cancer cell lines were purchased from the American Type Culture Collection (ATCC, Manassas, VA, USA). Cells were grown at 37℃ in 5% CO_2 in Iscove's Modified Dulbecco's Medium (IMDM; Invitrogen, Carlsbad, CA) supplemented with 10% fetal bovine serum (FBS; Invitrogen). Plasmids and siRNA were transfected using Lipofectamine 2000 (Invitrogen) and Lipofectamine RNAiMAX (Invitrogen), respectively. D4476, a CK-1 inhibitor, was used at a concentration of 100 μM (Abcam, Cambridge, UK).

Plasmid DNA and siRNA

To generate FAM83H–FLAG-expressing plasmid, cDNA encoding human *FAM83H* (NM_198488.3) was amplified from HCT116 cells by PCR using the forward primer 5′-ATAGAATTCAACATGGCCCGTCGCTCTCAGAG-3′ and the reverse primer 5′-ACGGGATCCTCCCTTCTTGCTTTTGAACG-3′ and cloned into the p3XFLAG-CMV-14 vector (Sigma-Aldrich, St Louis, MO). *FAM83H* cDNA from HCT116 cells has three silent mutations (1896C/T, 2001C/A and 2953C/T). To generate plasmids expressing FLAG-tagged N-terminal fragments of FAM83H (amino acids 1–286, FAM83H-286N–FLAG; 1–296, FAM83H-296N–FLAG), the corresponding regions of *FAM83H* cDNA were amplified by PCR using the common forward primer 5′-ATAGAATTCA-ACATGGCCCGTCGCTCTCAGAG-3′ and the reverse primer 5′-ATAG-GATCCGGGCACAAGCGGCTCGGACTG-3′ for FAM83H-286N–FLAG and 5′-ATAGGATCCGGCGTCCATGCGGGCCAG-3′ for FAM83H-296N–FLAG and cloned into the p3XFLAG-CMV-14 vector. FAM83H-251A–FLAG and FAM83H-274A–FLAG were generated using a PrimeSTAR Mutagenesis Basal Kit (Takara Bio, Shiga, Japan) and FAM83H–FLAG vector. For the 251A mutant, 5′-TGGTCCGCTGAGAAGATCCACCGCAGC-3′ and 5′-CTTCTCAGCGGA-CCACATGAAGCTGTA-3′ were used as PCR primers. For the 274A mutant, 5′-GAGGAGGCCCGCATCCTCTTCGCGCAG-3′ and 5′-GATGCGGGCCT-CCTCGTCGAAGCTGGA-3′ were used as PCR primers. FAM83H siRNAs (FAM83H siRNA S1, FAM83H-HSS138852; FAM83H siRNA S2, FAM83H-HSS138851) were purchased from Invitrogen. CK-1α siRNAs targeting the sequence 5′-CAGAATTTGCGATGTACTT-3′ or 5′-GAATTTGCGATGTACTT-AA-3′ and plectin siRNA targeting the sequence 5′-CCAAGAACTTGCA-GAAGTT-3′ were purchased from Sigma-Aldrich. The control siRNA duplexes were purchased from Invitrogen (Medium GC Duplex #2) and Sigma-Aldrich (Mission negative control SIC-001).

Antibodies

The following antibodies were purchased: anti-FAM83H (HPA024604; Sigma-Aldrich), anti-keratin-8 (TS1, Thermo Scientific, Fremont, CA; EP1628Y, Epitomics, Burlingame, CA), anti-keratin-18 (DC10; Thermo Scientific), anti-keratin 19 (RCK108; Thermo Scientific), anti-α-tubulin (DM1A, Sigma-Aldrich; YOL1/34, Santa Cruz Biotechnology, Santa Cruz, CA), anti-FLAG (M2; Sigma-Aldrich), anti-E-cadherin (36B5; Thermo Scientific), anti-CK-1α (C-19; Santa Cruz Biotechnology), anti-phospho-keratin-8-Ser431 (EP1630; Epitomics), anti-phospho-keratin-8-Ser73 (E431-2; Abcam), anti-phospho-keratin-18-Ser33 (sc-101727; Santa Cruz Biotechnology), anti-phospho-keratin-18-Ser52 (sc-17032; Santa Cruz Biotechnology), anti-plectin (sc-7572; Santa Cruz Biotechnology) and anti-actin (C-11; Santa Cruz Biotechnology). Mouse IgG1 control (MOPC-21; Exbio, Vestec, Czech Republic) was used for immunoprecipitation. Alexa Fluor 488 and Alexa Fluor 594 donkey anti-mouse IgG and Alexa Fluor 488 and Alexa Fluor 594 donkey anti-rabbit IgG, Alexa Fluor 488 donkey anti-goat IgG, and Alexa Fluor 488 donkey anti-rat IgG antibodies were used for immunofluorescence (Invitrogen). HRP-conjugated horse anti-mouse IgG (Cell Signaling Technology, Beverly, MA), donkey anti-rabbit IgG (GE Healthcare, Little Chalfont, UK), and donkey anti-goat IgG (Santa Cruz Biotechnology) antibodies were used for western blotting.

Tissue samples from colorectal cancer patients

Tumor and adjacent non-tumor tissue samples were collected from patients with colorectal cancer in the Department of Frontier Surgery, Chiba University Hospital. For qPCR, tissue samples were rapidly frozen and stored at −80℃. For immunofluorescence, tissue samples were embedded in OCT compound (Sakura Finetek, Tokyo, Japan), snap frozen in liquid nitrogen, and cut into 5 μm sections using a cryostat (Hyrax C50; Carl Zeiss, Jena, Germany). Paraffin-embedded blocks were cut into 2.5 μm sections using a microtome, REM-710 (Yamato, Saitama, Japan). The protocol for the collection and use of the tissue samples was

Journal of Cell Science

approved by the ethics committees of the Graduate School of Medicine, Chiba University and the Proteome Research Center, National Institute of Biomedical Innovation. Written informed consent was obtained from each patient before surgery.

Quantitative PCR

Extraction of total RNA and cDNA synthesis were performed as described previously (Tomonaga et al., 2004). qPCR reaction was performed using Power CYBR Green reagents (Applied Biosystems, Foster City, CA). The levels of mRNA encoding FAM83H and β-actin were examined, and the value of FAM83H was normalized by that of β-actin in each tissue sample. The following primer pairs were used: FAM83H, forward primer 5′-cgacaagtgccgtgtcaacc-3′ and reverse primer 5′-acttcccagtgcggcagtag-3′; β-actin, forward primer 5′-agaaaatctggcaccacacc-3′ and reverse primer 5′-ggggtgttgaaggtctcaaa-3′.

Protein extraction, immunoprecipitation and western blotting

For the extraction of whole cellular proteins of cell lines, cells were directly lysed in SDS-PAGE sample buffer. For preparation of cell lysates used for immunoprecipitation (IP lysates), cells were suspended in PBS containing 1% NP40, Complete protease inhibitor cocktail (Roche, Basel, Switzerland), and PhosSTOP phosphatase inhibitor cocktail (Roche), and then homogenized by sonication. After centrifugation at 100,000 ***g*** for 30 minutes, the supernatant was collected. Immunoprecipitation was performed using antibodies crosslinked to Protein G Dynabeads (Invitrogen) using dimethyl pimelimidate dehydrochloride (MP Biochemicals, Santa Ana, CA). IP lysates were reacted with antibody-coated Dynabeads for 1 hour at 4℃, and the absorbed proteins were eluted with 100 mM glycine-HCl (pH 3.0) or SDS-PAGE sample buffer. Western blotting was performed using the chemiluminescence detection system ECL or ECL Prime (GE Healthcare). The images were obtained with LAS4000 (Fuji Film, Tokyo, Japan) and processed with Multi Gauge V3.2 (Fuji Film) and Photoshop CS5 (Adobe, San Jose, CA).

Protein identification by LC-MS/MS

Immunoprecipitates with anti-FLAG antibody were resolved by SDS-PAGE and the gel lane was divided into nine pieces corresponding to different molecular masses. In-gel tryptic digestion of proteins was performed as described previously (Adachi et al., 2007). The digested peptides were analyzed using an LTQ-Orbitrap Velos mass spectrometer (Thermo Scientific) equipped with a nanoHPLC system (Paradigm MS2; Michrom, Auburn, CA) and an HTC-PAL autosampler (Zwingen, Kanton Bern, Switzerland). A 0.3×5 mm trap column [L-column ODS; Chemicals Evaluation and Research Institute (CERI), Tokyo, Japan] and an analytical column made in-house by packing L-column2 C18 (CERI) into a self-pulled needle (0.1×200 mm) were used (Muraoka et al., 2012; Narumi et al., 2012). The mobile phases consisted of buffer A (0.1% formic acid and 2% acetonitrile) and B (0.1% formic acid and 90% acetonitrile). The nanoLC gradient was delivered at 500 nl/minute and consisted of a linear gradient of buffer B developed from 5 to 35% B in 45 minutes. The dynamic exclusion function of LTQ-Orbitrap was turned off. For protein identification, peptide mass data were matched by searching the UniProtKB/Swiss-Prot database (2011_12) using the MASCOT search engine v2.3. Database search parameters were: the charge of the precursor ion, 2+ and 3+; peptide mass tolerance, 3 ppm; fragment tolerance, 0.6 Da; allowing up to one missed cleavage; fixed modification, carbamidomethylation of cysteine; variable modification, oxidation of methionine. Proteins were identified based on at least two unique peptides. The number of assigned spectra was calculated using Scaffold 3 software (Proteome Software, Portland, OR) for semi-quantitation.

Immunofluorescence and immunohistochemistry

Cells or tissue sections from snap-frozen tissues were fixed with methanol at −20℃ for 2 minutes or 4% paraformaldehyde in PBS at 30℃ for 20 minutes, permeabilized with 0.5% Triton X-100 in PBS for 5 minutes on ice, blocked in PBS containing 0.01% Tween 20 and 3% BSA on ice, and sequentially incubated with primary and secondary antibodies at room temperature. For immunofluorescence, DNA was stained with 100 ng/ml of 4′-6-diamidino-2-phenylindole (DAPI; Sigma-Aldrich) and stained samples were viewed under an LSM710 confocal microscope with Zen software (Carl Zeiss, Jena, Germany). The objective lenses were EC Plan-NEO FLUAR 10× /0.3 or 40× /1.3 and Plan APOCHROMAT 63× /1.4. Pearson's correlation coefficient was calculated using Zen software, according to the manufacturer's instructions. The value can range from 1 to −1, with 1 indicating a complete positive correlation, −1 a negative correlation and with 0 indicating no correlation. For immunohistochemistry, visualization was performed with diaminobenzidine (DAB) chromogen (EnVision+ Kit/HRP; Dako, Glostrup, Denmark) and nuclei were stained with Mayer's hematoxylin (Muto Pure Chemicals, Tokyo, Japan) (Seimiya et al., 2008). Stained sections were scanned on a NanoZoomer RS digital slide imaging system (Hamamatsu Photonics, Hamamatsu, Japan). Two pathologists evaluated the immunostaining of colorectal cancer tissues. Composite figures were prepared using Photoshop CS5.

Acknowledgements

We would like to thank Hiromi Saito, Masayoshi Kuwano, Shio Watanabe and Yuuki Hashimoto for technical assistance.

Author contributions

T.K. designed the study, performed experiments and prepared manuscript; T.T. designed the study and prepared the manuscript; H.K. contributed to the design of the study; I.H., T.N. and H.M. collected human tissue samples; N.K. gave technical support; J.A., M.S. and T.S. gave advice on the design of proteomic, pathological and biological experiments.

Funding

This work was supported by a Grant-in-Aid, Research on Biological Markers for New Drug Development [grant number H20-0005 to T.T.]; the Ministry of Health, Labour and Grants-in-Aids [grant numbers 21390354 to T.T. and 22790539 to T.K.]; the Ministry of Education, Science, Sports and Culture of Japan.

Supplementary material available online at
http://jcs.biologists.org/lookup/suppl/doi:10.1242/jcs.129684/-/DC1

References

Adachi, J., Kumar, C., Zhang, Y. and Mann, M. (2007). In-depth analysis of the adipocyte proteome by mass spectrometry and bioinformatics. *Mol. Cell. Proteomics* **6**, 1257-1273.

Ameen, N. A., Figueroa, Y. and Salas, P. J. (2001). Anomalous apical plasma membrane phenotype in CK8-deficient mice indicates a novel role for intermediate filaments in the polarization of simple epithelia. *J. Cell Sci.* **114**, 563-575.

Beil, M., Micoulet, A., von Wichert, G., Paschke, S., Walther, P., Omary, M. B., Van Veldhoven, P. P., Gern, U., Wolff-Hieber, E., Eggermann, J. et al. (2003). Sphingosylphosphorylcholine regulates keratin network architecture and visco-elastic properties of human cancer cells. *Nat. Cell Biol.* **5**, 803-811.

Birchmeier, W. and Behrens, J. (1994). Cadherin expression in carcinomas: role in the formation of cell junctions and the prevention of invasiveness. *Biochim. Biophys. Acta* **1198**, 11-26.

Boczonadi, V., McInroy, L. and Määttä, A. (2007). Cytolinker cross-talk: periplakin N-terminus interacts with plectin to regulate keratin organisation and epithelial migration. *Exp. Cell Res.* **313**, 3579-3591.

Bühler, H. and Schaller, G. (2005). Transfection of keratin 18 gene in human breast cancer cells causes induction of adhesion proteins and dramatic regression of malignancy in vitro and in vivo. *Mol. Cancer Res.* **3**, 365-371.

Elyada, E., Pribluda, A., Goldstein, R. E., Morgenstern, Y., Brachya, G., Cojocaru, G., Snir-Alkalay, I., Burstain, I., Haffner-Krausz, R., Jung, S. et al. (2011). CKIα ablation highlights a critical role for p53 in invasiveness control. *Nature* **470**, 409-413.

Flitney, E. W., Kuczmarski, E. R., Adam, S. A. and Goldman, R. D. (2009). Insights into the mechanical properties of epithelial cells: the effects of shear stress on the assembly and remodeling of keratin intermediate filaments. *FASEB J.* **23**, 2110-2119.

Hatanaka, H., Takada, S., Tsukui, M., Choi, Y. L., Kurashina, K., Soda, M., Yamashita, Y., Haruta, H., Hamada, T., Tamada, K. et al. (2010). Identification of the transforming activity of Indian hedgehog by retroviral expression screening. *Cancer Sci.* **101**, 60-64.

Izawa, I. and Inagaki, M. (2006). Regulatory mechanisms and functions of intermediate filaments: a study using site- and phosphorylation state-specific antibodies. *Cancer Sci.* **97**, 167-174.

Kim, J. W., Lee, S. K., Lee, Z. H., Park, J. C., Lee, K. E., Lee, M. H., Park, J. T., Seo, B. M., Hu, J. C. and Simmer, J. P. (2008). FAM83H mutations in families with autosomal-dominant hypocalcified amelogenesis imperfecta. *Am. J. Hum. Genet.* **82**, 489-494.

Klammer, M., Kaminski, M., Zedler, A., Oppermann, F., Blencke, S., Marx, S., Müller, S., Tebbe, A., Godl, K. and Schaab, C. (2012). Phosphosignature predicts dasatinib response in non-small cell lung cancer. *Mol. Cell. Proteomics* **11**, 651-668.

Knippschild, U., Gocht, A., Wolff, S., Huber, N., Löhler, J. and Stöter, M. (2005). The casein kinase 1 family: participation in multiple cellular processes in eukaryotes. *Cell. Signal.* **17**, 675-689.

Knösel, T., Emde, V., Schlüns, K., Schlag, P. M., Dietel, M. and Petersen, I. (2006). Cytokeratin profiles identify diagnostic signatures in colorectal cancer using multiplex analysis of tissue microarrays. *Cell. Oncol.* **28**, 167-175.

Kölsch, A., Windoffer, R., Würflinger, T., Aach, T. and Leube, R. E. (2010). The keratin-filament cycle of assembly and disassembly. *J. Cell Sci.* **123**, 2266-2272.

Lee, S. K., Hu, J. C., Bartlett, J. D., Lee, K. E., Lin, B. P., Simmer, J. P. and Kim, J. W. (2008). Mutational spectrum of FAM83H: the C-terminal portion is required for tooth enamel calcification. *Hum. Mutat.* **29**, E95-E99.

Liu, Y. H., Cheng, C. C., Ho, C. C., Chao, W. T., Pei, R. J., Hsu, Y. H., Ho, L. C., Shiu, B. H. and Lai, Y. S. (2011). Plectin deficiency on cytoskeletal disorganization and transformation of human liver cells in vitro. *Med. Mol. Morphol.* **44**, 21-26.

Journal of Cell Science

Long, H. A., Boczonadi, V., McInroy, L., Goldberg, M. and Määttä, A. (2006). Periplakin-dependent re-organisation of keratin cytoskeleton and loss of collective migration in keratin-8-downregulated epithelial sheets. *J. Cell Sci.* **119**, 5147-5159.
Miller, R. K., Vikstrom, K. and Goldman, R. D. (1991). Keratin incorporation into intermediate filament networks is a rapid process. *J. Cell Biol.* **113**, 843-855.
Miller, R. K., Khuon, S. and Goldman, R. D. (1993). Dynamics of keratin assembly: exogenous type I keratin rapidly associates with type II keratin in vivo. *J. Cell Biol.* **122**, 123-135.
Moll, R., Divo, M. and Langbein, L. (2008). The human keratins: biology and pathology. *Histochem. Cell Biol.* **129**, 705-733.
Muraoka, S., Kume, H., Watanabe, S., Adachi, J., Kuwano, M., Sato, M., Kawasaki, N., Kodera, Y., Ishitobi, M., Inaji, H. et al. (2012). Strategy for SRM-based verification of biomarker candidates discovered by iTRAQ method in limited breast cancer tissue samples. *J. Proteome Res.* **11**, 4201-4210.
Narumi, R., Murakami, T., Kuga, T., Adachi, J., Shiromizu, T., Muraoka, S., Kume, H., Kodera, Y., Matsumoto, M., Nakayama, K. et al. (2012). A strategy for large-scale phosphoproteomics and SRM-based validation of human breast cancer tissue samples. *J. Proteome Res.* **11**, 5311-5322.
Okamura, H., Garcia-Rodriguez, C., Martinson, H., Qin, J., Virshup, D. M. and Rao, A. (2004). A conserved docking motif for CK1 binding controls the nuclear localization of NFAT1. *Mol. Cell. Biol.* **24**, 4184-4195.
Omary, M. B., Ku, N. O., Tao, G. Z., Toivola, D. M. and Liao, J. (2006). "Heads and tails" of intermediate filament phosphorylation: multiple sites and functional insights. *Trends Biochem. Sci.* **31**, 383-394.
Omary, M. B., Ku, N. O., Strnad, P. and Hanada, S. (2009). Toward unraveling the complexity of simple epithelial keratins in human disease. *J. Clin. Invest.* **119**, 1794-1805.
Oriolo, A. S., Wald, F. A., Ramsauer, V. P. and Salas, P. J. (2007). Intermediate filaments: a role in epithelial polarity. *Exp. Cell Res.* **313**, 2255-2264.
Osmanagic-Myers, S., Gregor, M., Walko, G., Burgstaller, G., Reipert, S. and Wiche, G. (2006). Plectin-controlled keratin cytoarchitecture affects MAP kinases involved in cellular stress response and migration. *J. Cell Biol.* **174**, 557-568.
Pankov, R., Simcha, I., Zöller, M., Oshima, R. G. and Ben-Ze'ev, A. (1997). Contrasting effects of K8 and K18 on stabilizing K19 expression, cell motility and tumorigenicity in the BSp73 adenocarcinoma. *J. Cell Sci.* **110**, 965-974.
Polakis, P. (2000). Wnt signaling and cancer. *Genes Dev.* **14**, 1837-1851.
Salas, P. J., Rodriguez, M. L., Viciana, A. L., Vega-Salas, D. E. and Hauri, H. P. (1997). The apical submembrane cytoskeleton participates in the organization of the apical pole in epithelial cells. *J. Cell Biol.* **137**, 359-375.
Sasaroli, D., Gimotty, P. A., Pathak, H. B., Hammond, R., Kougioumtzidou, E., Katsaros, D., Buckanovich, R., Devarajan, K., Sandaltzopoulos, R., Godwin, A. K. et al. (2011). Novel surface targets and serum biomarkers from the ovarian cancer vasculature. *Cancer Biol. Ther.* **12**, 169-180.
Seimiya, M., Tomonaga, T., Matsushita, K., Sunaga, M., Oh-Ishi, M., Kodera, Y., Maeda, T., Takano, S., Togawa, A., Yoshitomi, H. et al. (2008). Identification of novel immunohistochemical tumor markers for primary hepatocellular carcinoma; clathrin heavy chain and formiminotransferase cyclodeaminase. *Hepatology* **48**, 519-530.
Sivaramakrishnan, S., Schneider, J. L., Sitikov, A., Goldman, R. D. and Ridge, K. M. (2009). Shear stress induced reorganization of the keratin intermediate filament network requires phosphorylation by protein kinase C zeta. *Mol. Biol. Cell* **20**, 2755-2765.
Steinert, P. M., Idler, W. W. and Zimmerman, S. B. (1976). Self-assembly of bovine epidermal keratin filaments in vitro. *J. Mol. Biol.* **108**, 547-567.
Strnad, P., Windoffer, R. and Leube, R. E. (2001). In vivo detection of cytokeratin filament network breakdown in cells treated with the phosphatase inhibitor okadaic acid. *Cell Tissue Res.* **306**, 277-293.
Strnad, P., Windoffer, R. and Leube, R. E. (2002). Induction of rapid and reversible cytokeratin filament network remodeling by inhibition of tyrosine phosphatases. *J. Cell Sci.* **115**, 4133-4148.
Thiery, J. P., Acloque, H., Huang, R. Y. and Nieto, M. A. (2009). Epithelial-mesenchymal transitions in development and disease. *Cell* **139**, 871-890.
Tomonaga, T., Matsushita, K., Yamaguchi, S., Oh-Ishi, M., Kodera, Y., Maeda, T., Shimada, H., Ochiai, T. and Nomura, F. (2004). Identification of altered protein expression and post-translational modifications in primary colorectal cancer by using agarose two-dimensional gel electrophoresis. *Clin. Cancer Res.* **10**, 2007-2014.
Urzúa, B., Ortega-Pinto, A., Morales-Bozo, I., Rojas-Alcayaga, G. and Cifuentes, V. (2011). Defining a new candidate gene for amelogenesis imperfecta: from molecular genetics to biochemistry. *Biochem. Genet.* **49**, 104-121.
Valenta, T., Hausmann, G. and Basler, K. (2012). The many faces and functions of β-catenin. *EMBO J.* **31**, 2714-2736.
Wiche, G. (1998). Role of plectin in cytoskeleton organization and dynamics. *J. Cell Sci.* **111**, 2477-2486.
Windoffer, R. and Leube, R. E. (1999). Detection of cytokeratin dynamics by time-lapse fluorescence microscopy in living cells. *J. Cell Sci.* **112**, 4521-4534.
Windoffer, R., Wöll, S., Strnad, P. and Leube, R. E. (2004). Identification of novel principles of keratin filament network turnover in living cells. *Mol. Biol. Cell* **15**, 2436-2448.
Windoffer, R., Beil, M., Magin, T. M. and Leube, R. E. (2011). Cytoskeleton in motion: the dynamics of keratin intermediate filaments in epithelia. *J. Cell Biol.* **194**, 669-678.
Wöll, S., Windoffer, R. and Leube, R. E. (2007). p38 MAPK-dependent shaping of the keratin cytoskeleton in cultured cells. *J. Cell Biol.* **177**, 795-807.
Wright, J. T., Frazier-Bowers, S., Simmons, D., Alexander, K., Crawford, P., Han, S. T., Hart, P. S. and Hart, T. C. (2009). Phenotypic variation in FAM83H-associated amelogenesis imperfecta. *J. Dent. Res.* **88**, 356-360.
Yano, T., Tokui, T., Nishi, Y., Nishizawa, K., Shibata, M., Kikuchi, K., Tsuiki, S., Yamauchi, T. and Inagaki, M. (1991). Phosphorylation of keratin intermediate filaments by protein kinase C, by calmodulin-dependent protein kinase and by cAMP-dependent protein kinase. *Eur. J. Biochem.* **197**, 281-290.

Journal of Cell Science

EXPERIMENTAL CELL RESEARCH 319 (2013) 3251–3268

Available online at www.sciencedirect.com

ScienceDirect

journal homepage: www.elsevier.com/locate/yexcr

Research Article

Formation of long and winding nuclear F-actin bundles by nuclear c-Abl tyrosine kinase

Kazumasa Aoyama[a], *Ryuzaburo Yuki*[a], *Yasuyoshi Horiike*[a], *Sho Kubota*[a], *Noritaka Yamaguchi*[a], *Mariko Morii*[a], *Kenichi Ishibashi*[a], *Yuji Nakayama*[a], *Takahisa Kuga*[b], *Yuuki Hashimoto*[b], *Takeshi Tomonaga*[b], *Naoto Yamaguchi*[a,*]

[a]*Department of Molecular Cell Biology, Graduate School of Pharmaceutical Sciences, Chiba University, Inohana 1-8-1, Chuo-ku, Chiba 260-8675, Japan*

[b]*Laboratory of Proteome Research, National Institute of Biomedical Innovation, Ibaraki, Osaka 567-0085, Japan*

ARTICLE INFORMATION

Article Chronology:
Received 20 May 2013
Received in revised form
9 August 2013
Accepted 6 September 2013
Available online 13 September 2013

Keywords:
c-Abl tyrosine kinase
Tyrosine phosphorylation
Nucleus
Actin-biding domain
Actin dynamics
F-actin

ABSTRACT

The non-receptor-type tyrosine kinase c-Abl is involved in actin dynamics in the cytoplasm. Having three nuclear localization signals (NLSs) and one nuclear export signal, c-Abl shuttles between the nucleus and the cytoplasm. Although monomeric actin and filamentous actin (F-actin) are present in the nucleus, little is known about the relationship between c-Abl and nuclear actin dynamics. Here, we show that nuclear-localized c-Abl induces nuclear F-actin formation. Adriamycin-induced DNA damage together with leptomycin B treatment accumulates c-Abl into the nucleus and increases the levels of nuclear F-actin. Treatment of c-Abl-knockdown cells with Adriamycin and leptomycin B barely increases the nuclear F-actin levels. Expression of nuclear-targeted c-Abl (NLS-c-Abl) increases the levels of nuclear F-actin even without Adriamycin, and the increased levels of nuclear F-actin are not inhibited by inactivation of Abl kinase activity. Intriguingly, expression of NLS-c-Abl induces the formation of long and winding bundles of F-actin within the nucleus in a c-Abl kinase activity-dependent manner. Furthermore, NLS-c-AblΔC, which lacks the actin-binding domain but has the full tyrosine kinase activity, is incapable of forming nuclear F-actin and in particular long and winding nuclear F-actin bundles. These results suggest that nuclear c-Abl plays critical roles in actin dynamics within the nucleus.

© 2013 Elsevier Inc. All rights reserved.

Introduction

Non-receptor-type tyrosine kinases act as cytoplasmic signaling molecules and play important roles in various cellular events, such as cell proliferation, differentiation, migration, and apoptosis. The non-receptor-type tyrosine kinase c-Abl is composed of a Src homology (SH) 3 domain, an SH2 domain, a kinase catalytic domain, and the unique last exon region. The last exon region is important for the localization and functions of c-Abl, because it contains three nuclear localization signals (NLSs), a nuclear export signal (NES), a DNA-binding domain, and an actin-binding domain [1,2]. The c-Abl actin-binding domain consists of the monomeric actin (globular actin, G-actin)- and polymeric actin (filamentous actin, F-actin)-binding domains, which cooperatively bundle F-actin in vitro [3]. Cytoplasmic c-Abl is known to play roles in actin dynamics, including actin polymerization and F-actin assembly, in the cytoplasm [4,5].

*Corresponding author. Fax: +81 43 226 2868.
E-mail address: nyama@faculty.chiba-u.jp (N. Yamaguchi).

0014-4827/$ - see front matter © 2013 Elsevier Inc. All rights reserved.
http://dx.doi.org/10.1016/j.yexcr.2013.09.003

Several tyrosine kinases and phosphatases are involved in nuclear events [6,7]. Our previous studies showed that Lyn, a member of non-receptor-type Src-family tyrosine kinases (SFKs), is present in the nucleus although Lyn does not seem to have any NLSs [8–10]. Nuclear localization of Lyn is enhanced by inhibition of its kinase activity, Crm1-dependent nuclear export or lipid modifications [9]. Unlike SFKs, c-Abl has three NLSs and an NES, which enable c-Abl to shuttle between the cytoplasm and the nucleus [11]. DNA damage stimulates nuclear translocation of c-Abl, and nuclear c-Abl is involved in DNA damage responses through its activation mediated by ATM-dependent phosphorylation [12–15].

Actin, a major component of the cytoskeleton, is highly abundant in the cytoplasm. Nonetheless, actin, in both monomeric and polymeric

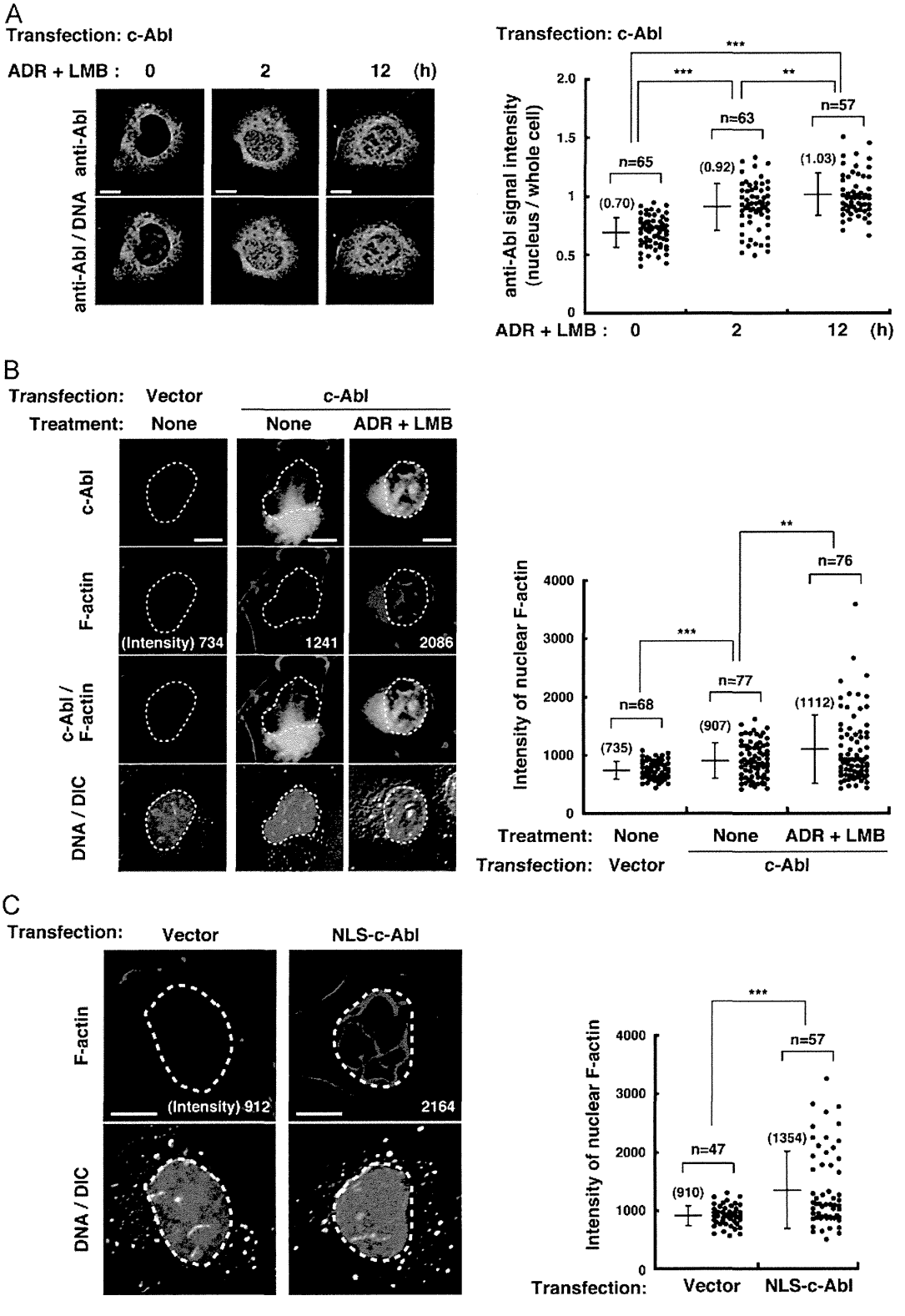

forms, is shown to exist in the nucleus [16–21] possibly through active export and import [22–25]. Although c-Abl has NLSs and the actin-binding domain, the relationship between c-Abl and nuclear actin is poorly understood.

In this study, we showed the involvement of nuclear c-Abl in nuclear F-actin formation, which is independent of c-Abl tyrosine kinase activity but dependent on the c-Abl actin-binding domain. We also showed that tyrosine phosphorylation mediated by nuclear c-Abl induces formation of long and winding nuclear F-actin bundles in a manner dependent on the c-Abl actin-binding domain. The extent of the formation of nuclear F-actin bundles was positively correlated with the level of nuclear F-actin. These results suggest that nuclear c-Abl plays a critical role in nuclear F-actin formation.

Materials and methods

Plasmids

cDNA encoding human wild-type c-Abl-1b (c-Abl) (provided by E. Canaani; [26]) was subcloned into the pcDNA4/TO vector (Invitrogen), as described previously [27]. NLS-c-Abl was constructed and subcloned into the pcDNA4/TOneo vector as described recently [28]. NLS-c-AblΔC was constructed from pcDNA4/TOneo-NLS-c-Abl with Apa I digestion, blunting, and ligation. NLS-Lyn-HA (NLS-Lyn) and NLS-Syk were constructed from cDNA encoding human wild-type Lyn (provided by Yamamoto [29]) and Syk (provided by Clark [30]) as described previously [10]. The pEGFP-β-actin vector and the EGFPpENTR4/H1 vector were provided by Bito [31] and Miyoshi, respectively. The mCherry-β-actin vector was constructed, as described [32].

Antibodies

The following antibodies were used: phosphotyrosine (pTyr) (4G10 and polyclonal antibody: Upstate Biotechnology, Inc; provided by Tamura and Yoshimoto [33]), Abl (8E9; BD-Pharmingen), Lyn (H-6; Santa Cruz Biotechnology), Syk (4D10; Santa Cruz Biotechnology), FLAG (M2 and polyclonal antibody; Sigma), α-tubulin (MCA78G; Serotec), lamin A/C (Santa Cruz Biotechnology). Horseradish peroxidase (HRP)-F(ab′)$_2$ secondary antibodies were purchased from Amersham Bioscience. TRITC-IgG, and Alexa Fluor 488- and Alexa Fluor 647-IgG secondary antibodies were purchased from BioSource International, Sigma-Aldrich, and Invitrogen.

Cells and transfection

HeLa (Japanese Collection of Research Bioresources, Osaka), COS-1, NIH3T3 cells, and NLS-c-Abl-inducible cells (HeLa S3/TR/NLS-c-Abl; [28]) were cultured in Iscove's modified DME containing 5% bovine serum (BS) or 4% BS plus 1% fetal bovine serum (FBS). To generate a c-Abl knockdown cell line (COS-1/shAbl), COS-1 cells were co-transfected with a plasmid encoding the hygromycin-resistance gene and a plasmid encoding short hairpin RNA

Fig. 1 – Formation of nuclear F-actin bundles by nuclear c-Abl (A, B) COS-1 cells transfected with vector alone or c-Abl were cultured for 24 h in the presence of 1 μg/ml Adriamycin (ADR) and 5 ng/ml leptomycin B (LMB) during the last 0, 2, or 12 h. (A) Cells were fixed with methanol at −20 °C for 5 min, and doubly stained with anti-Abl antibody and propidium iodide (PI). Scale bars, 10 μm. The levels of nuclear localization of c-Abl were assessed by measuring a ratio of mean fluorescence intensity of anti-Abl staining in the nucleus to that in the corresponding whole cell (nucleus/whole cell). The plot represents the level of nuclear localization of c-Abl in each cell, and bars represent means ± S.D. from a representative experiment. Numbers in parentheses indicate mean values, and asterisks indicate the significant difference (*$p<0.001$) calculated by Student's *t*-test. n, cell number. (B) Cells were extracted with Triton extraction buffer containing 0.4% paraformaldehyde at 4 °C for 3 min, fixed with 4% paraformaldehyde, and triply stained with anti-Abl antibody, Alexa Fluor 647-phalloidin, and PI. The resulting red emission of PI-stained DNA is pseudo-colored as blue. Differential–interference–contrast, DIC. Scale bars, 10 μm. Broken lines indicate the outline of the nucleus. The plot represents the mean fluorescence intensity of phalloidin staining in each nucleus, and bars represent means ± S.D. from a representative experiment. Numbers in parentheses indicate mean values, and asterisks indicate the significant difference (**$p<0.01$; ***$p<0.001$) calculated by Student's *t*-test. (C) COS-1 cells transfected with vector alone or NLS-c-Abl were cultured for 24 h. Cells were extracted and fixed as described in (B), and triply stained with anti-FLAG antibody for NLS-c-Abl, Alexa Fluor 647-phalloidin, and PI. Scale bars, 10 μm. The level of nuclear F-actin in each nucleus was plotted as described in (B). Asterisks indicate the significant difference (***$p<0.001$) calculated by Student's *t*-test. (D) COS-1 cells transfected with vector alone, c-Abl, or NLS-c-Abl were cultured for 24 h in the presence or absence of 1 μg/ml ADR and 5 ng/ml LMB during the last 2 or 12 h. Cells were extracted and fixed as described in (B), and triply stained with Alexa Fluor 448-phalloidin, anti-lamin A/C antibody, and anti-pTyr antibody. Z-section images (thickness, 0.6 μm) of a representative cell at 2.0-μm intervals (*Z* axis) from the lowest (0 μm) to the highest (8 μm) position are shown. Scale bars, 10 μm. The levels of nuclear F-actin and lamin A/C in each nucleus were quantitated in the image at 4 μm from the bottom of the cells (0 μm). Results were plotted as described in (B). Asterisks indicate the significant difference (*$p<0.05$; **$p<0.01$; ***$p<0.001$; NS, not significant) calculated by Student's *t*-test. (E) COS-1 cells transfected with vector alone or NLS-c-Abl were cultured for 24 h in the presence of DMSO, 1 μg/ml latrunculin B (Lat B), or 1 μg/ml nocodazole (Noc) during the last 1 h. Cells were extracted, fixed and stained, as described in Fig. 1C. Scale bars, 10 μm. (F) COS-1 cells cotransfected with GFP-β-actin plus NLS-c-Abl or GFP-β-actin plus vector alone were cultured for 24 h and extracted with 0.1% TritonX-100 in PBS without fixation. Scale bars, 10 μm. (G) COS-1 cells transfected with NLS-c-Abl were cultured for 24 h. Cells were extracted and fixed as described in (B), and stained with Alexa Fluor 488-phalloidin. Z-section images of a representative cell at 0.9-μm intervals (*Z* axis) from the lowest (0 μm) to the highest (8.1 μm) position are shown. The Z-section images are merged in a two-dimensional image (Merge). Scale bar, 10 μm. (H) COS-1 cells transfected with vector alone or NLS-c-Abl were cultured for 24 h. Cells were extracted and fixed as described in (B), and stained with anti-FLAG antibody, Alexa Fluor 647-phalloidin, and PI. Scale bars, 10 μm. Nuclear F-actin bundle formation was shown with the level of nuclear F-actin (intensity).**

(shRNA) against c-Abl, which was generated from EGFP/pENTR4/H1/shAbl by NcoI and EcoRI digestion and blunting to delete the EGFP gene, and selected in 500 μg/ml hygromycin. EGFP/pENTR4/H1/shAbl was generated by subcloning shRNA for silencing c-Abl (5′-GGATCAACACTGCTTCTGAT-3′) [34] into the EGFP/pENTR4/H1 vector, as described recently [28]. Cells seeded in a 35-mm (60-mm) culture dish were transiently transfected with 1 μg (3 μg) of plasmid DNA using 5 μg (15 μg) of linear polyethylenimine

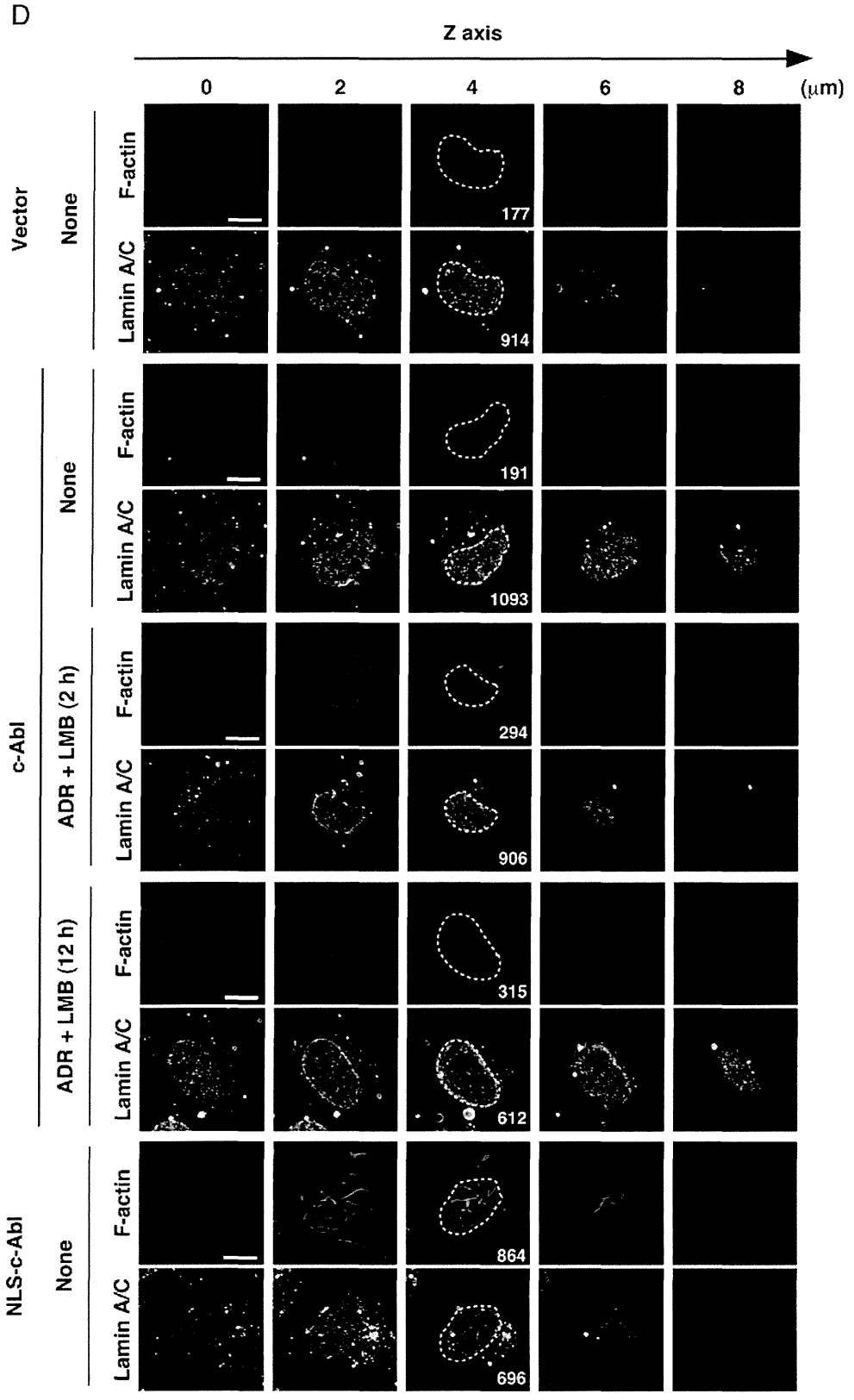

Fig. 1 – (*continued*)

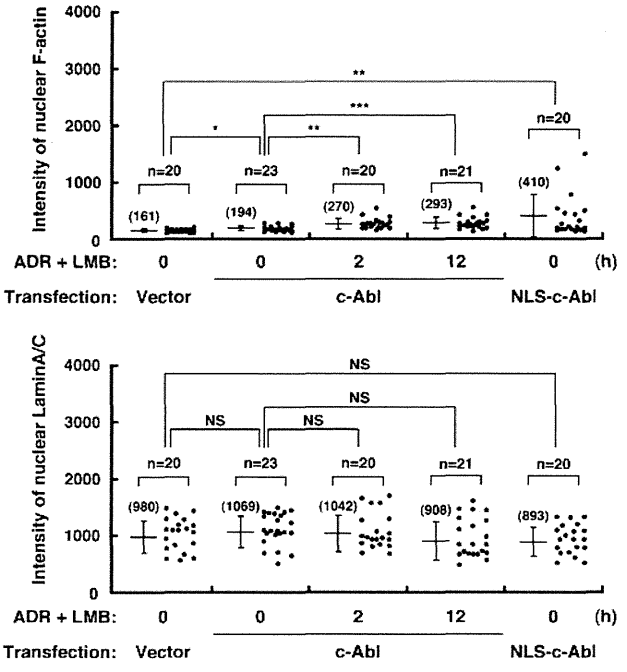

Fig. 1 – (*continued*)

(25 kDa) (Polyscience, Inc.) [35]. For nuclear accumulation of c-Abl, cells were treated for 2 or 12 h with 1 μg/ml Adriamycin (ADR) (Sigma-Aldrich) as a DNA-damaging agent and 5 ng/ml leptomycin B (LMB) (LC Laboratories) as an inhibitor of Crm1-mediated nuclear export. c-Abl-mediated tyrosine phosphorylation was verified by treatment with 10 μM imatinib (Abl inhibitor; LC Laboratories), 10 μM PP2 (SFK inhibitor; Calbiochem), 20 μM U0126 (MEK inhibitor; Merck), or 100 nM wortmannin (PI3K inhibitor; Alomone Labs). For depolymerization of F-actin and microtubules, cells were treated with 1 μg/ml latrunculin B (LatB) (Enzo Life Sciences) and 1 μg/ml nocodazole (Noc) (Sigma), respectively.

Immunofluorescence

Confocal and Nomarski differential-interference-contrast (DIC) images were obtained using a Fluoview FV500 confocal laser scanning microscope with a 40 × 1.00 N.A. dry or a 60 × 1.00 N.A. water-immersion objective (Olympus, Tokyo) and an LSM510 or an LSM700 laser scanning microscope with a 63 × 1.40 N.A. oil immersion objective (Carl Zeiss), as described [9,10,32,36–39]. One planar (*xy*) section slice was shown in all experiments, unless otherwise noted. Slice thickness: 0.6 μm (Figs. 1D, F, 2C

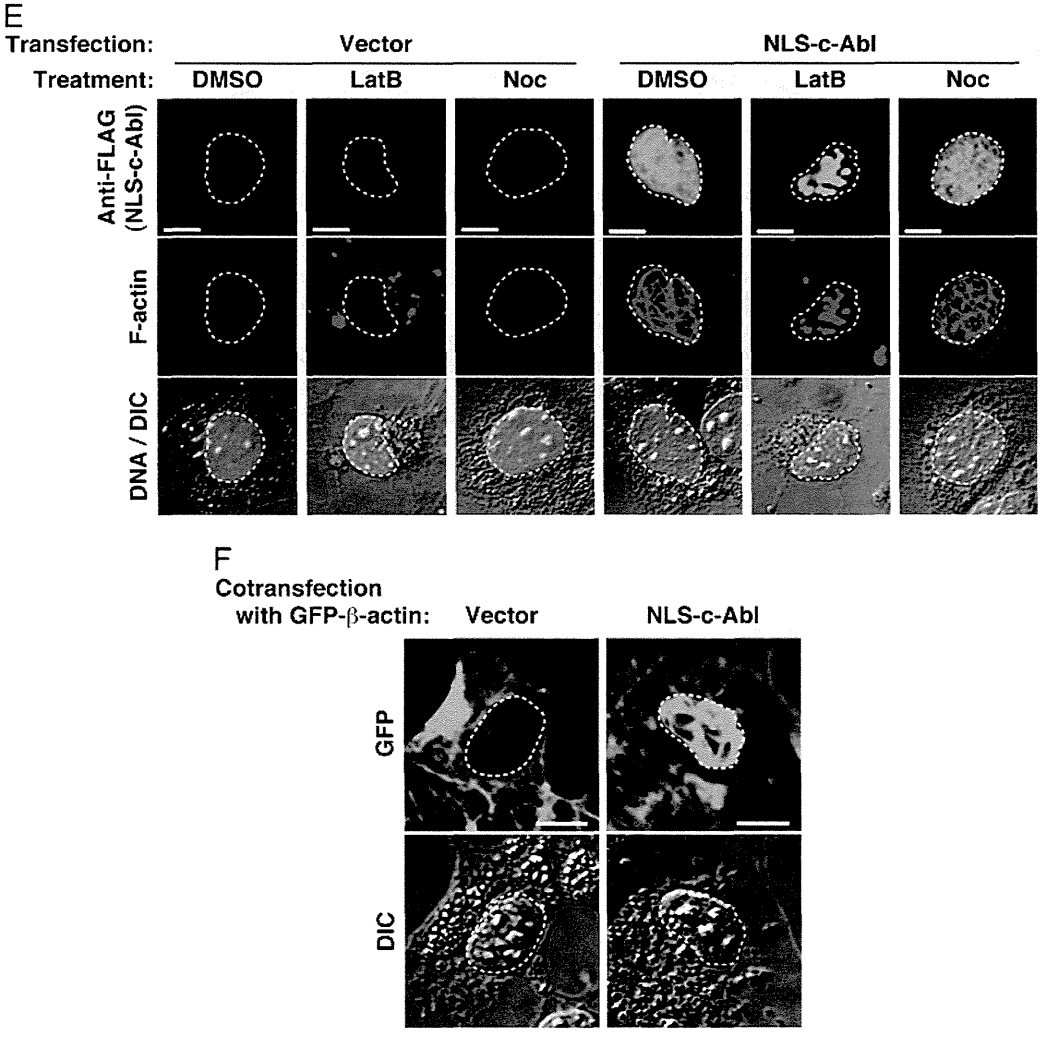

Fig. 1 – (*continued*)

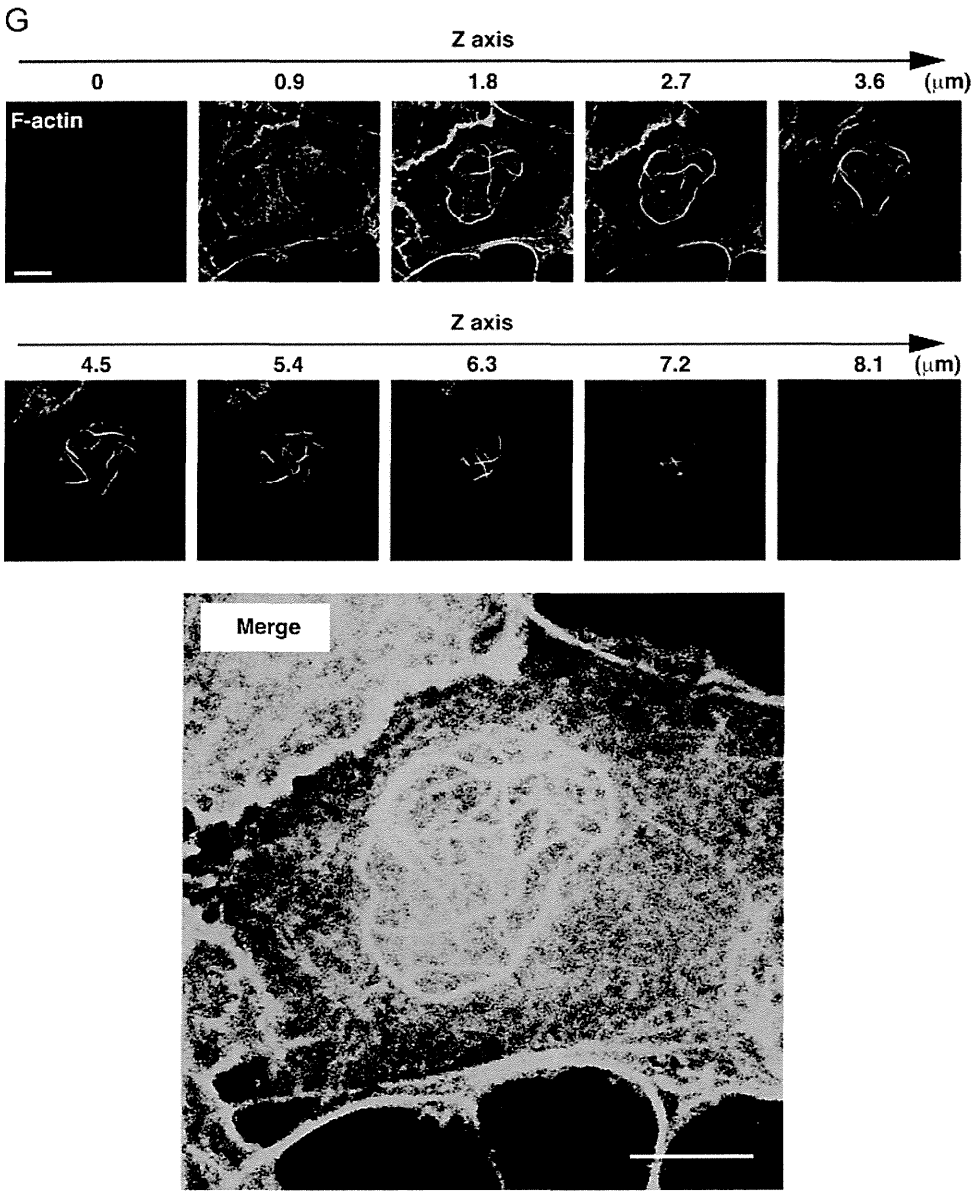

Fig. 1 – (*continued*)

and 5E), 0.7 μm (Figs. 1G and 5F), 1.0 μm (Fig. 1A), and 2.0 μm (Figs. 1B, C, E, H, 2B, 3A–D, 4A, 5C and D). In brief, cells were extracted in Triton extraction buffer (0.1% Triton X-100, 10 mM PIPES, pH 6.8, 100 mM NaCl, 300 mM sucrose, and 3 mM $MgCl_2$) containing 0.4% paraformaldehyde at 4 °C for 3 min before fixation with 4% paraformaldehyde, and permeabilized in phosphate-buffered saline (PBS) containing 0.1% saponin and 3% bovine serum albumin at room temperature [40,41]. Cells were subsequently reacted with an appropriate primary antibody for 1 h, washed with PBS containing 0.1% saponin, and stained with TRITC-, Alexa Fluor 488- or Alexa Fluor 647-conjugated secondary antibody for 1 h. For F-actin staining, cells were treated with Alexa Fluor 488- or 647-conjugated phalloidin (Invitrogen) for 1 h. For DNA staining, cells were treated with 200 μg/ml RNase A and 2–20 μg/ml propidium iodide (PI) for 1 h. After staining, cells were mounted in *p*-phenylenediamine-PBS-glycerin solution.

Quantitation of c-Abl nuclear localization and nuclear F-actin bundle formation

Confocal images were obtained as described above. For quantitation of the levels of c-Abl nuclear localization, a ratio of mean fluorescence intensity of anti-Abl staining in the nucleus to that in the corresponding whole cell (nucleus / whole cell) was measured using the ImageJ software (National Institutes of Health), as described previously [28]. For quantitation of nuclear F-actin formation, mean values of integrated fluorescence intensities of phalloidin staining in individual nuclei were measured using the ImageJ software.

Western blotting

Western blotting was performed with enhanced chemiluminescence (Millipore) as described previously [8,9,37,38,42–44].

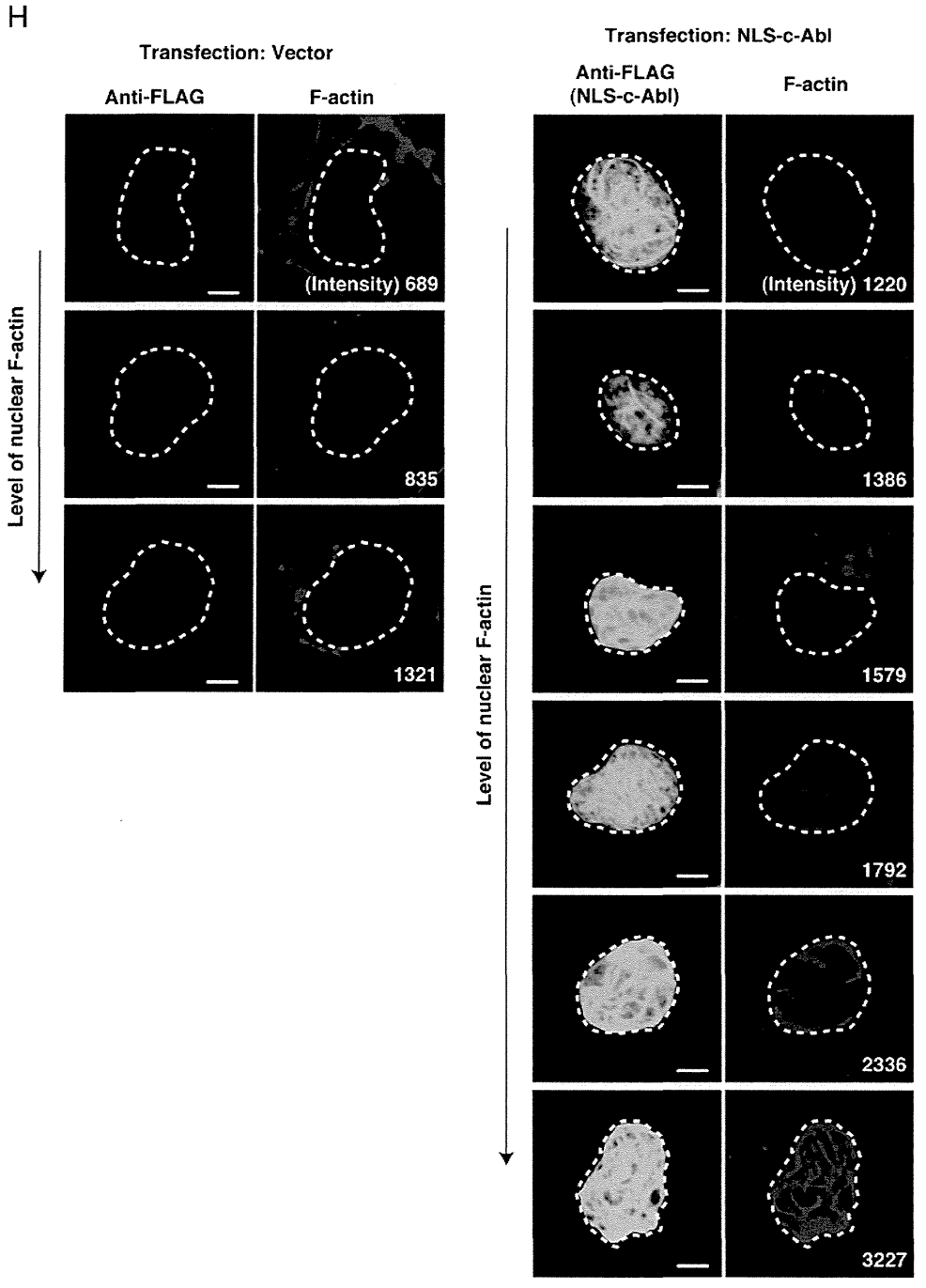

Fig. 1 – (*continued*)

Whole cell lysates prepared in SDS-sample buffer were subjected to SDS-polyacrylamide gel electrophoresis and electrotransferred onto polyvinylidene difluoride membranes. Protein bands were detected with appropriate antibodies and analyzed using a ChemiDoc XRSPlus image analyzer (Bio-Rad). Sequential reprobing of membranes with a variety of antibodies was performed after inactivation of HRP by 0.1% NaN_3, according to the manufacturer's instructions. Composite figures were prepared using Gimp version 2.6.2 software and Illustrator 14.0 software (Adobe).

Detection of c-Abl-mediated tyrosine phosphorylation in the nucleus

HeLa S3/TR/NLS-c-Abl cells [28] were treated with 1 μg/ml doxycycline (Dox) and cultured for 24 h to express NLS-c-Abl. Because tyrosine phosphorylation was hardly detected irrespective of the addition of Dox, HeLa S3/TR/NLS-c-Abl cells treated with Dox were incubated with 0.5 mM Na_3VO_4 during the last 1 h to minimize dephosphorylation by protein-tyrosine phosphatases [45]. To further inhibit protein-tyrosine phosphatases, cells were